Synthesis of Novel c(AmpRGD)-Sunitinib Dual Conjugates as Molecular Tools Targeting the $\alpha_v\beta_3$ Integrin/VEGFR2 Couple and Impairing Tumor-Associated Angiogenesis

Andrea Sartori,[a] Elisabetta Portioli,[a] Lucia Battistini,[a] Lido Calorini,[b] Alberto Pupi,[b,c] Federica Vacondio,[a] Daniela Arosio,[d] Francesca Bianchini,[b,c] and Franca Zanardi*[a]*

[a] Dipartimento di Farmacia, Università degli Studi di Parma, Parco Area delle Scienze 27A, 43124 Parma, Italy

[b] Dipartimento di Scienze Biomediche, Sperimentali e Cliniche "Mario Serio", Università degli Studi di Firenze, Viale G. B. Morgagni 50, 50134 Firenze, Italy

[c] Centro Interdipartimentale per lo Sviluppo Preclinico dell'Imaging Molecolare (CISPIM), Università degli Studi di Firenze, Viale G. B. Morgagni 50, 50134 Firenze, Italy

[d] Istituto di Scienze e Tecnologie Molecolari, Consiglio Nazionale delle Ricerche, Via Golgi 19, 20133 Milano, Italy

KEYWORDS: Angiogenesis, Dual conjugates, Growth Factor Receptors, Integrins, RGD Ligands, Peptidomimetics, Sunitinib

ABSTRACT

Based on a previously discovered anti-$\alpha_V\beta_3$ integrin peptidomimetic – c(AmpRGD) – and the clinically approved anti-angiogenic kinase inhibitor sunitinib, three novel dual conjugates were synthesized (compounds **1**-**3**), featuring the covalent and robust linkage between these two active modules. In all conjugates, the ligand binding competence toward $\alpha_V\beta_3$ (using both isolated receptors and $\alpha_V\beta_3$-overexpressing endothelial progenitor EP cells) and the kinase inhibitory activity (toward both isolated kinases and EPCs) remained almost untouched and comparable to the activity of the single active units. Compounds **1**-**3** showed interesting anti-angiogenesis properties in vitro via tubulogenesis assays; furthermore, dimeric-RGD conjugate **3** strongly inhibited angiogenesis in vivo during preliminary Matrigel plug assays in implanted FVB mice. These results offer proof-of-concept of how the covalent conjugation of two angiogenesis-related small modules may result in novel and stable molecules, which impair tumor-related angiogenesis with equal or even superior ability as compared to the single modules or their simple combinations.

INTRODUCTION

Targeted therapy that selectively addresses oncogenic drivers,[1-3] as well as the use of drugs concomitantly perturbing multiple molecular targets and signaling pathways[4-6] are arising as privileged therapeutic options. Angiogenesis, the process by which new blood vessels arise from preexisting vasculature, plays crucial roles in both normal and pathological events. In particular, aberrant angiogenesis – involving constantly activated vasculature – is widely accepted as a key player in a variety of pathological conditions including cancer growth and metastasis, rheumatoid

arthritis and age-related macular degeneration. Many diverse endogenous molecular systems participate in the angiogenesis regulation, including pro-angiogenic vascular endothelial growth factors (VEGFs), platelet-derived growth factors (PDGFs), their associated tyrosine kinase receptors (VEGFRs and PDGFRs), matrix metalloproteinases (MMPs), ephrin-ephrin receptor complexes, and specific extracellular matrix (ECM)-recognizing integrin receptors as $\alpha_V\beta_3$, $\alpha_V\beta_5$ and $\alpha_5\beta_1$.[7-12]

Substantial four decade-long body of research in this field resulted in worldwide approval by drug agencies of effective anti-angiogenic drugs including the humanized monoclonal antibodies trastuzumab and bevacizumab, which are VEGF antagonists, and several small molecules such as sunitinib and sorafenib, which mainly target the highly conserved cytosolic tyrosine kinase domain of VEGFRs.[9,12] Sunitinib, in particular (Figure 1), is an alkylidene 2-oxindole agent which acts as a highly effective multitarget tyrosine kinase inhibitor (TKI, mainly against VEGFR2, PDGFRβ, cKit, and Flt-3);[13-16] it is indicated as first-line therapy for metastatic renal cell carcinoma, pancreatic neuroendocrine tumors, second-line therapy for imatinib-resistant gastrointestinal stromal tumors,[13-16] and it is still the focus of countless clinical trials.[17]

Among antiangiogenic $\alpha_V\beta_3$-integrin inhibitors, the small molecule cilengitide [c(RGD)NMefV] is the most widely studied, and several advanced clinical trials are still in progress concerning the use of this drug as either single agent or in combination with radiotherapy.[18-21] However, the limited long-term efficacy and the systemic toxicity associated with the clinical use of the approved anti-angiogenic drugs posed serious concerns about the actual benefit and safety of these treatments.[22-29]

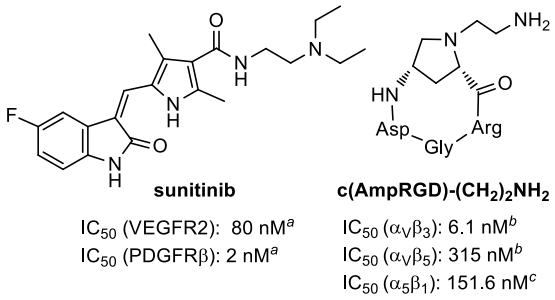

Figure 1. The antiangiogenic drug sunitinib and the 4-aminoproline-based RGD cyclotetrapeptide c(AmpRGD)-$(CH_2)_2NH_2$. [a]Ref. 13; [b]Ref. 42; [c]Ref. 43.

While the debate about the actual usefulness of anti-angiogenesis therapy remains open,[22-29] current researches suggest that possible solutions could entail the use of drugs capable of hitting multiple targets/pathways and cell types involved in the tumor microenvironment,[10,12,25,29,30] while possessing supplemental selective targeting moieties.

Among the intricate, often overlapping cell signaling networks regulating angiogenesis, growing evidence emerged for strict crosstalk between the VEGFR2 and $\alpha_V\beta_3$ receptors.[31-36] These two receptors are physically and functionally connected in common cell populations (e.g. endothelial cells, ECs, and several cancer cell types) and their interactions are important for both integrin activation and mutual regulation of the kinase activity.[31-36] Blockage of the $\alpha_V\beta_3$/VEGFR2 couple may thus be of high therapeutic potential.[37-40] In fact, the combined use of two small molecules – cilengitide and the sunitinib analogue SU5416 (Figure 2, A) – showed anti-angiogenic effect and inhibition of tumor melanoma growth and metastasis during in vivo preclinical studies.[37] In this instance, however, the two drugs were independently delivered, with possible differences in localization and pharmacokinetics. In an enlightening study,[38] a dual

specific scVEGF protein was engineered, capable of binding the extracellular portions of $\alpha_V\beta_3$ and VEGFR2 simultaneously, showing promise for effective in vitro and in vivo anti-angiogenic action (Figure 2, B). Though highly promising, this work had the limitation of dealing with complex engineered 25 kDa-weighty proteins.

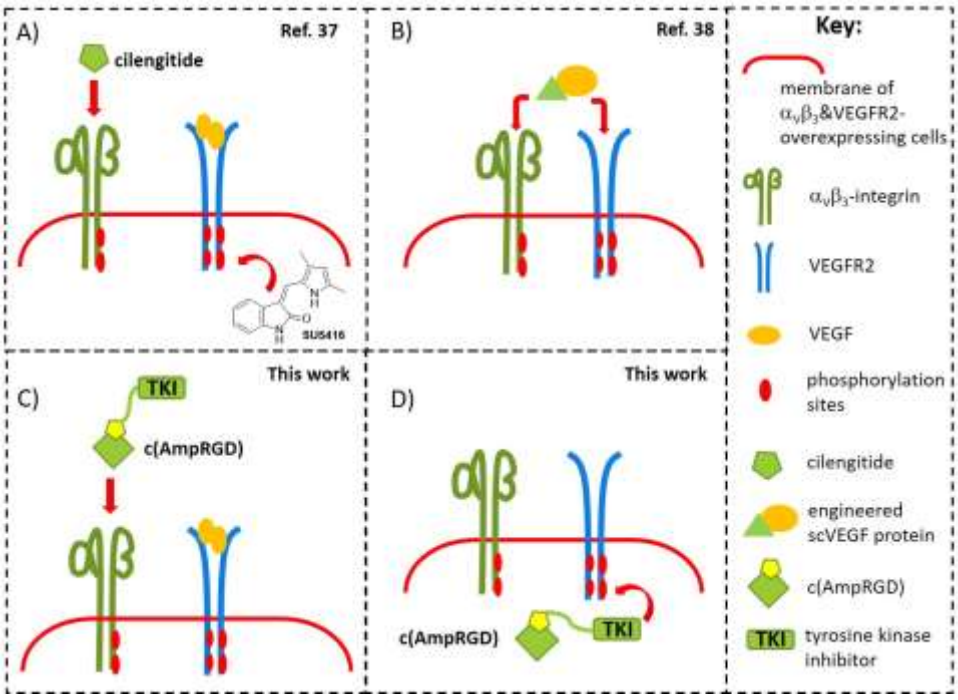

Figure 2. A) $\alpha_V\beta_3$ antagonist cilengitide (outside cell)+VEGFR2 antagonist (inside), two discrete small molecules, different localization (Ref. 37); B) one engineered dual-specific protein (outside), simultaneous $\alpha_V\beta_3$/VEGFR2 inhibition (Ref. 38); C) and D) one small molecule, the c(AmpRGD)-TKI conjugate, recognizing $\alpha_V\beta_3$ (outside), partially entering the cell (possibly via $\alpha_V\beta_3$), and antagonizing VEGFR2 (inside) (this work).

A complementary and conceptually different approach is here proposed, according to which a selective binder of the extracellular segment of $\alpha_V\beta_3$ is covalently linked to a proven TKI such as sunitinib, whose interaction with the cytoplasmic domain of VEGFR2 is widely recognized. As $\alpha_V\beta_3$ binder, we could rely on a recently discovered series of aminoproline-based RGD cyclotetrapeptides of type c(AmpRGD)-$(CH_2)_2NH_2$ (Figure 1)[41-43] which showed remarkable and selective binding capability toward the $\alpha_V\beta_3$ integrin receptor in both cell-free and cell assays. The covalent assemblage of an anchorable sunitinib-like moiety to the c(AmpRGD) portion through a suitable linker would furnish dual conjugates (Figure 2 C and 2 D, schematic representation) wherein the RGD unit would possibly provide *i*) EC-selective targeting by $\alpha_V\beta_3$-RGD recognition, *ii*) $\alpha_V\beta_3$-dependent anti-angiogenic effect, and *iii*) $\alpha_V\beta_3$-mediated cell internalization. On the other hand, the sunitinib unit could exert its intracellular TKI effect after internalization, while playing a role in overall perturbation of the $\alpha_V\beta_3$-VEGFR2 crosstalk.[44-46]

We herein disclose the design, synthesis, and biological activity evaluation of three novel covalent prototypes **1**-**3** (Figure 3). In particular, the binding properties toward $\alpha_V\beta_3$ integrin, kinase inhibitory activity, cell uptake, and anti-angiogenesis potential in vitro and in vivo are reported and discussed, vis-à-vis the behavior of the single modules and their simple combinations.

RESULTS AND DISCUSSION

Design of cAmpRGD-sunitinib Conjugates. To fulfill the objectives of this work (Figure 2 C and 2 D), the projected dual conjugates had to embody several stringent requisites. First, *the*

active units should not disturb each other, that is, the sunitinib moiety should not compromise the RGD-binding capability while the RGD unit should not impede the tyrosine kinase activity of sunitinib. Second, to *exclude premature detachment* of the two active units (outside the targeted cells), the linker between them should be either uncleavable or cleaved within cells exclusively; and third, *the conjugate must enter the targeted cells* possibly via $\alpha_V\beta_3$-mediated endocytosis.

As a background, extensive structure-activity relationship studies on sunitinib analogues[13,47] and X-ray analysis of the complex between the drug and the tyrosine kinase domain of the VEGFR2 active site[48,49] revealed that the aromatic portion of the molecule is directly involved in the binding, while the terminal tertiary amine stands outside the pocket and may allow certain margins of structural modifications. Thus, connection of sunitinib to the linker exploiting this amine terminal would likely be uninfluential toward the tyrosine kinase activity. Furthermore, we were aware of the binding capability and selectivity toward the $\alpha_V\beta_3$ integrin of c(AmpRGD)-based ligands and related conjugates,[41-43,50,51] anticipating that conjugation of these ligands with the ancillary sunitinib moiety would not hardly compromise their $\alpha_V\beta_3$-integrin binding ability. Lastly, the cell internalization potential of c(AmpRGD)-conjugates was preliminarily assayed using a c(AmpRGD)-fluorescein conjugate control which demonstrated complete $\alpha_V\beta_3$-dependent internalization in A375 melanoma cells within 25 min exposure (see details in the Supporting Information).

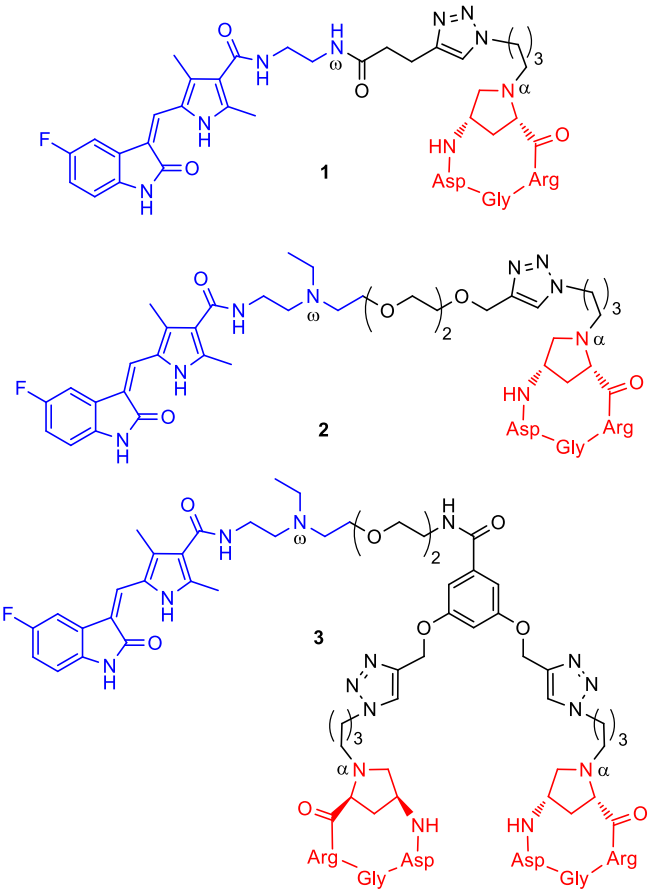

Figure 3. Structure of the targeted dual conjugates **1**-**3**.

With these clues at hand, conjugates **1**-**3** were designed, wherein the two active units are positioned 11-to-22 bonds away (Figure 3, N^{α} to N^{ω}) and are connected via robust triazole/ether/amide linkages, as shown in Figure 3. Monomeric compounds **1** and **2** differ from each other in the linker length and type; compounds **2** and **3** share a common pegylated linker and maintain the tertiary amine functionality of the parent drug, while compound **1** replaces this amine with a secondary amide. Finally, compound **3** features a dimeric RGD presentation, which could be important for enhanced integrin recognition and integrin-mediated cell internalization.[52-57]

Chemistry. The synthesis began with the preparation of three constitutive modules namely, the c(AmpRGD)-azide **7** (Scheme 1), the sunitinib analogue **13** (Scheme 2), and the linker moieties **14**, **16**, and **18** (Scheme 3 and Supporting Information). Thus, commercially available protected *cis*-amino-L-proline **4** was selectively deprotected at the *N*(α)-site and alkylated via reductive amination using 4-azidopropanal (Scheme 1).

Scheme 1. Synthesis of the c(AmpRGD) Modules 7 and 8[a]

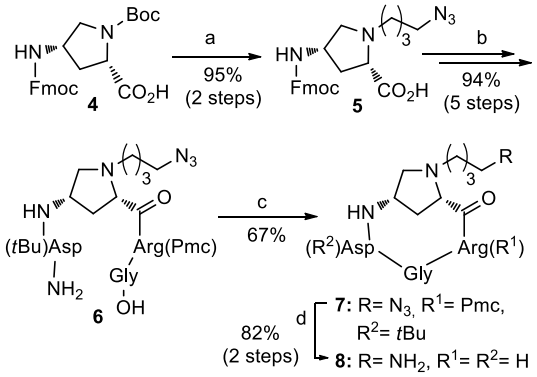

[a]Reagents and conditions: (a) (i) TFA, DCM, rt; (ii) 4-azidobutanal, $NaBH(OAc)_3$, 1,2-DCE, rt; (b) *Fmoc-SPPS*: (i) Cl-cTrt-O-Gly-(Pmc)Arg-NH_2, **5**, HATU, HOAt, collidine, DMF, rt; (ii) piperidine, DMF, rt; (iii) Fmoc-Asp(*t*BuO)-OH, HATU, HOAt, collidine, DMF, rt; (iv) piperidine, DMF, rt; (v) AcOH, TFE, DCM, rt; (c) HATU, HOAt, collidine, DCM/DMF, rt; (d) (i) H_2, Pd/C, EtOH, rt; (ii) TFA/TIS/H_2O (95:2.5:2.5), rt.

Azidoproline **5** was efficiently obtained (95% yield), and inserted into the projected peptide chain via conventional Fmoc-based solid phase peptide synthesis (Fmoc-SPPS) using chlorotrityl (cTrt) resin. After detachment from the resin, **6** was recovered in 94% yield and subjected to in-solution cyclization under diluted conditions (13:1 DCM/DMF solvent mixture, 2.2 mM), using

the HATU/HOAt reagent couple, giving protected azido-terminating cyclotetrapeptide **7**, ready for the subsequent conjugation step. Overall, the novel azide module **7** was prepared in a eight-step sequence and rewarding 63% overall yield from proline **4**. Azide **7** could be also conveniently converted to free amine **8** via reduction and acidic deprotection (82%, two steps), which served as a reference control during the biological assays (vide infra). It is to be noted that the synthesis of similar c(AmpRGD) azide/amine congeners possessing two carbon-long alkyl chains instead of four was reported by us in previous works;[42,43] in that instances, however, longer linear sequences were experienced (14-15 steps) and lower yields were obtained (10-16% overall yields).

Scheme 2. Synthesis of the Sunitinib-Like Module 13[a]

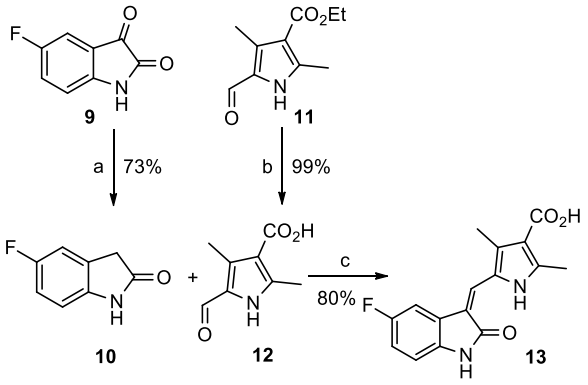

[a]Reagents and conditions: (a) NH_2NH_2, 100 °C; (b) KOH, H_2O, MeOH, reflux; (c) piperidine, EtOH, 60 °C.

As for the sunitinib portion, carboxylic acid **13** was judged a good precursor. As shown in Scheme 2, Knoevenagel condensation between oxindole **10**, in turn obtained from commercial 5-fluoroisatin **9** by Wolff-Kishner reduction, and pyrrole acid **12** (from saponification of the

corresponding commercial ethyl ester **11**) consigned 3-alkylidene 2-oxindole **13** in a good 80% yield,[13] as the sole detectable *Z*-configured isomer.[58]

Simple chemistry was used to access alkyne-terminating amine **14**, pegylated counterpart **16**, and bis-alkyne amine **18** (structures in Scheme 3), whose straightforward preparation from commercial starting materials is described in the Supporting Information.

All was ready for preparation of the three dual conjugates **1**-**3**, where the main modules could be connected through common synthesis pathways. Thus, as shown in Scheme 3, parallel BOP-promoted condensation of carboxylic acid **13** with either amines **14**, **16** or **18** provided access to the respective alkyne-terminating amides **15**, **17**, or **19** in good isolated yields (64-88%). Copper-catalyzed 1,3-dipolar cycloaddition between these alkynes and the previous c(AmpRGD) azide **7** (two-fold equivalents in case of the dimeric execution in eq. 3) followed by acidic deprotection gave conjugates **1**-**3** in good yields and purity after semipreparative reverse-phase HPLC purification (43-70% yields; 96-98% purity, recovered as TFA salts).

Scheme 3. Modular Synthesis of the Sunitinib-c(AmpRGD) Conjugates 1-3[a]

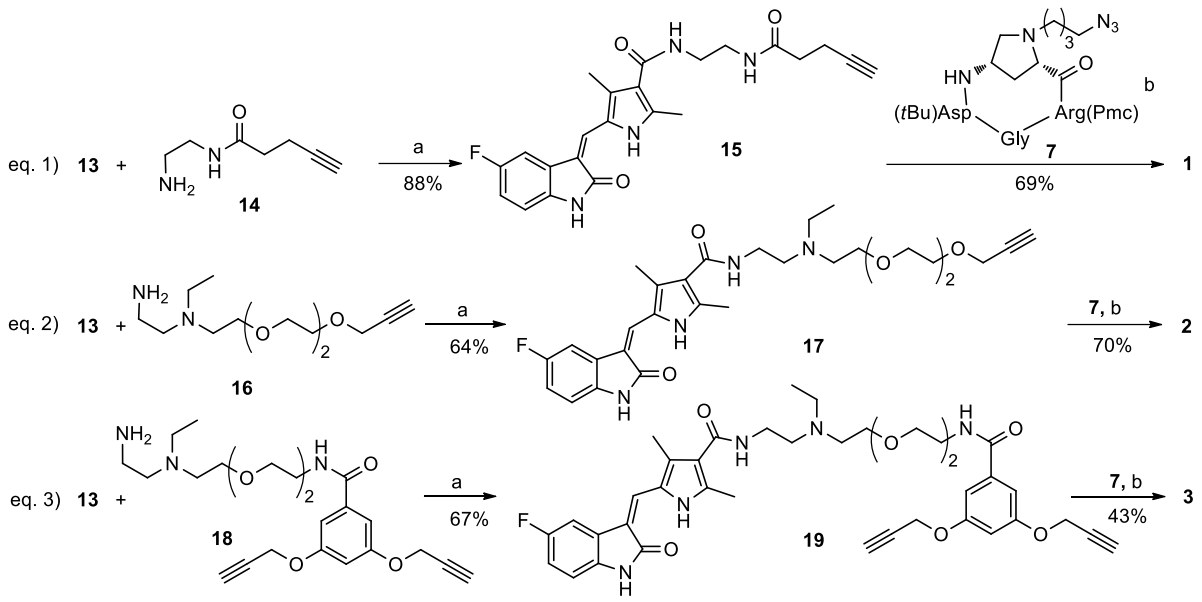

[a]Reagents and conditions: (a) BOP, DIPEA, DCM/DMF (2:3), rt; (b) (i) azide **7**, $Cu(OAc)_2$, Na L-asc, H_2O/DMF, rt; (ii) TFA/TIS/H_2O (95:2.5:2.5), rt.

In Vitro Stability of Conjugates 1-3. The in vitro stability of conjugates **1-3** in 80% v/v rat and human plasma was firstly evaluated by HPLC-UV-Vis analysis. The cyclopeptides were incubated and analyzed up to 8 h, as detailed in Table 1 (see also the Supporting Information). Invariably and regardless their intimate structure, compounds **1-3** showed complete resistance to rat and human plasma degradation during the observed time. This demonstrated that the covalent connection of the modules resulted in robust conjugates anticipating that, whatever the biological response, it would be the result of the interaction of the cell environment with the integral, preserved structure of the conjugates and not the individual detached components. Whether this would translate into a benefit or disadvantage in biological assays remained to be seen.

Table 1. In Vitro Plasma Stability of Compounds 1-3 vs Sunitinib

Compound	Rat plasma (% compd at 8h)[a]	Human plasma (% compd at 8h)[a]
sunitinib	97.3 (±9.1)	102.3 (±5.2)
1	88.2 (±12.7)	99.0 (±10.9)
2	104.1 (±3.3)	106.6 (±11.5)
3	108.8 (±10.5)	98.6 (±15.4)

[a]Percentage of compound remaining after 8 h of incubation in 80% v/v plasma, 37 °C, protected from light. Reported are Means ± SD.

Lipophilicity and Cellular Uptake of Conjugates 1-3. At physiological pH, compounds **1**-**3** proved highly hydrophilic in accordance with the measured negative values of the Log$D_{oct,7.4}$ (i.e. the distribution coefficient in *n*-octanol/buffer at pH 7.4, Table 2). As expected, attachment of the c(AmpRGD) module to the sunitinib-like portion turned the lipophilic character of the drug to hydrophilic, which was magnified by the pegylated linker (compounds **2** and **3** vs **1**) and the dipeptide presentation (**3** vs **1** and **2**).

Table 2. Lipophilicity and Cellular Uptake of Compounds 1-3 and Sunitinib in EPCs

Compound	Log $D_{oct,7.4}$[a]	MW	Intracellular Content (nmol/mg prot) (1 h)[b]	Cell uptake (pmol/min /mg prot) (1 h)	Log Cell Uptake (1 h)	Intracellular Content (nmol/mg prot) (8 h)[b]
sunitinib	2.51	398.5	5.72 (±0.71)	95.3	1.98	2.90 (±0.40)
1	– 2.03	960.0	0.26 (±0.02)	4.3	0.64	0.22 (±0.02)
2	– 2.56	1078.2	0.48 (±0.07)	8.0	0.90	0.43 (±0.09)
3	– 3.02	1788.9	0.94 (±0.02)	15.7	1.19	0.54 (±0.03)

[a]Distribution coefficient in the n-octanol/buffer system, pH 7.4. Reported are Means ± SD. [b]EPCs were incubated with 1μM final concentration of test compound. After 1 h, the medium containing the tested compounds was removed and intracellular content was quantified immediately and after 8 h. Experiments were conducted in triplicate and data were expressed as nmol/mg of total cell proteins in each sample.

The capability of endothelial progenitor cells (EPCs) to internalize conjugates **1**-**3** as compared to free sunitinib was next investigated. Total intracellular concentrations of **1**-**3** and sunitinib were measured by HPLC-ESI-MS/MS. EPCs were incubated in standard conditions for 1 h in the presence of the different compounds at 1 μM final concentration (see also Experimental and Figure S1 in the Supporting Information). As illustrated in Table 2, all compounds were detected in the intracellular extracts, with the small-sized sunitinib drug showing maximum levels at 1 h, while conjugates **1**-**3** were found in the cell extract to a much lesser extent. In particular, compound **1** showed a scarce entrance in cells after 1 h treatment, which remained almost

invariable after 8 h. Pegylated counterpart **2**, having similar molecular weight, almost doubled its ability to enter cells as compared to **1** at both 1 h and 8 h treatment. Finally, dimeric RGD conjugate **3**, notwithstanding its higher molecular weight, showed a 4-fold and 2-fold ability to enter cells as compared to **1** and **2**, respectively.

These data are quite interesting since they emphasize the following points: *i*) the requisite delivery of the sunitinib-like moiety inside cells is provided by conjugates **1**-**3**, even if the internalization is not as efficient as the free drug, and *ii*) the amount of each conjugate (expressed as pmol/min/mg prot) which passes through the EPC membrane in the first hour is, on a log scale, inversely related to its lipophilicity, expressed by the distribution coefficient at pH 7.4, *i.e.* Log(cell uptake) = -0.55(±0.04)log $D_{oct,\ 7.4}$ – 0.50(±0.10); n=3; r^2 = 0.995; s=0.03; F=191. The more hydrophilic and bulkier **3** is more efficiently internalized than **1**; the dependence of the internalized content upon the RGD presentation (monomeric vs dimeric) suggests a direct involvement of the RGD moiety during the internalization process possibly via $\alpha_V\beta_3$-mediated endocytosis.[52-57] The assay was repeated for compounds **2** and **3** in the presence of excess $\alpha_V\beta_3$ integrin ligand **8** (100 μM). Significant decrease of cell uptake was witnessed for both compounds (Table S1 in the Supporting Information) further corroborating the notion of an active role of this integrin during internalization.

Solid-phase receptor binding assay. The integrin activity and selectivity profile of compounds **1**-**3** were firstly evaluated by measuring their ability to bind to human, isolated $\alpha_V\beta_3$ and $\alpha_5\beta_1$ integrin receptors by competitive displacement assays using either biotinylated vitronectin VN (for $\alpha_V\beta_3$) or biotinylated fibronectin FN (for $\alpha_5\beta_1$). To better evaluate the impact of the sunitinib moiety on binding capability, the results were compared to those obtained for the

unconjugated counterpart c(AmpRGD)-$(CH_2)_2NH_2$ and commercial ligand c(RGDfV). As shown in Table 3, compounds **1**-**3** exhibited one-digit nanomolar affinity toward $\alpha_V\beta_3$ integrin, which was even superior to the unconjugated AmpRGD-based counterpart and showed in all cases an appreciable $\alpha_V\beta_3/\alpha_5\beta_1$ selectivity. Compound **3**, bearing a 2-fold RGD repeat, showed an increased binding affinity as compared to monomer **2**, even if it was lower than **1**. Overall, the presence of a sunitinib-linker cargo attached to the integrin-recognizing RGD unit did not compromise the exquisite binding affinity and selectivity of these conjugates.

Table 3. Inhibition of Biotinylated VN and FN Binding to $\alpha_V\beta_3$ and $\alpha_5\beta_1$ Receptors, Respectively[a]

Compound	IC_{50} (nM)±SD for $\alpha_V\beta_3$	IC_{50} (nM)±SD for $\alpha_5\beta_1$
1	1.24±0.01	30.7±17.7
2	5.1±0.6	101.3±31.3
3	3.8±0.6	95.8±46.7
c(AmpRGD)-$(CH_2)_2NH_2$	6.1±1.6[b]	151.6±67.6[b]
C(RGDfV)	3.2±1.3[b]	166.0±28.0[c]

[a]IC_{50} values were calculated as the concentration of compound required for 50% inhibition of biotinylated VN or FN binding to human, isolated receptors. Each data point represents the average of triplicate wells; data analysis was carried out by nonlinear regression analysis using GraphPad Prism software. Each experiment was repeated in duplicate. [b]Ref. 42. [c]Ref. 43.

Inhibition of EPC adhesion to the $\alpha_V\beta_3$-ligand vitronectin using conjugates 1-3. The synthesized compounds **1**-**3** were evaluated for their ability to inhibit the adhesion of natural ligand VN to $\alpha_V\beta_3$-overexpressing cells. Endothelial progenitor cells were chosen due to their abundant $\alpha_V\beta_3$ integrin receptor expression (as certified by flow cytometric analysis, Figure S2) and for their recognized role in tumor angiogenesis.[59-61] The assay of adhesion inhibition was

performed in the presence of 2.0 mmol/L $MnCl_2$ to switch $\alpha_v\beta_3$ integrin to its activated form with increasing concentrations of compounds **1**, **2** and **3** (1, 10, 100, 1000, 10000 nM); for comparison purposes, sunitinib alone, unconjugated c(AmpRGD) **8**, and a combination of both were also assayed.

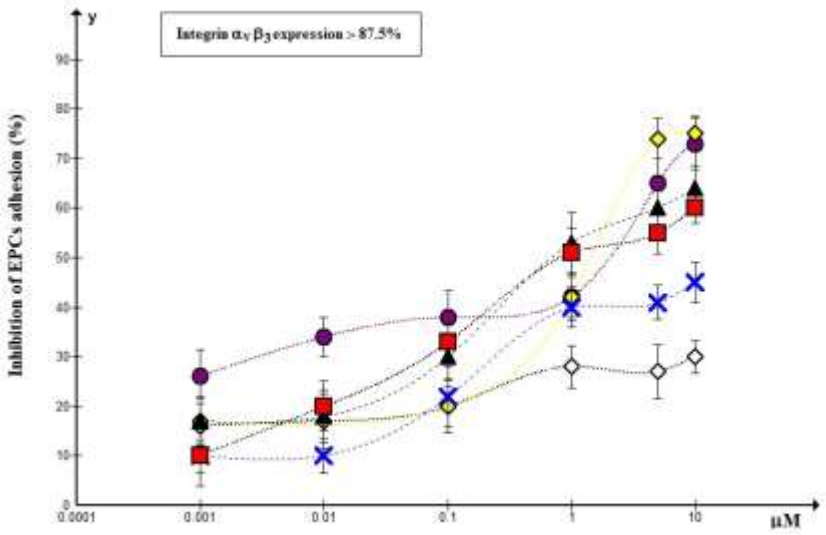

Figure 4. Inhibition of EPCs adhesion to VN in the presence of compounds **1**-**3**, **8**, sunitinib, and the combination sunitinib+**8** (▲ compound **1;** ✖ compound **2;** ■ compound **3;** ● compound **8;** ◇ sunitinib; ◆ compound **8**+sunitinib**)**. Top insert indicates the percentage of $\alpha_V\beta_3$ integrin expression in EPCs. The inhibitory activity was calculated as percentage of cell adhesion to VN in untreated cells and was expressed as mean±SD. Experiments were carried out in triplicate.

As shown in Figure 4, conjugated cyclopeptides **1** and **3** strongly inhibited cell adhesion in a dose-related manner with IC_{50} values nearly approaching 500 nM, while conjugate **2** showed a

less efficient activity (IC_{50} *ca* 10 μM); notably, the binding capability of compounds **1** and **3** was even better than the unconjugated counterpart **8** (IC_{50} 1.8 μM). As expected, the binding capability of sunitinib alone remained negligible at these concentrations. Overall, the covalent conjugation of the c(AmpRGD) portion to the sunitinib-like moiety as described in the diverse topologies of compounds **1**-**3** does not significantly alter the ligand binding capability towards these endothelial $\alpha_v\beta_3$-overexpressing cells.

Effect of conjugates 1-3 on cell proliferation and cell viability. The effect of the different compounds was evaluated on EPCs in a proliferation assay performed in the presence of VEGF-A (20 ng/mL), and the various compounds **1**-**3**, **8**, sunitinib, and **8**+sunitinib at 1 μM concentration every 24 h. The effect was followed after 24 h, 48 h and 72 h exposure. Cell proliferation was measured by cell count and cell viability was evaluated using trypan blue exclusion assay (Figure 5). After the first 24 h treatment, conjugates **1**-**3** showed inhibition of VEGF-induced proliferation of 46%, 24%, and 41%, respectively, with respect to untreated cells. On the other hand, sunitinib inhibited cell proliferation of 33%, and the combination of sunitinib with compound **8** poorly impacted cell proliferation. After 48 h treatment, conjugates **1**-**3** and sunitinib alone maintained almost the same level of inhibition of proliferation. Interestingly, the combination of sunitinib and compound **8** revealed a 23% of inhibition. After 72 h, inhibition of EPCs proliferation found in cells treated with compound **3** was similar to that of cells exposed to sunitinib, while other treatments did not show a significant inhibition of proliferation.

During the entire experiment, cell viability was monitored and no significant difference was found in EPCs exposed either to the conjugated compounds or to separate drugs.

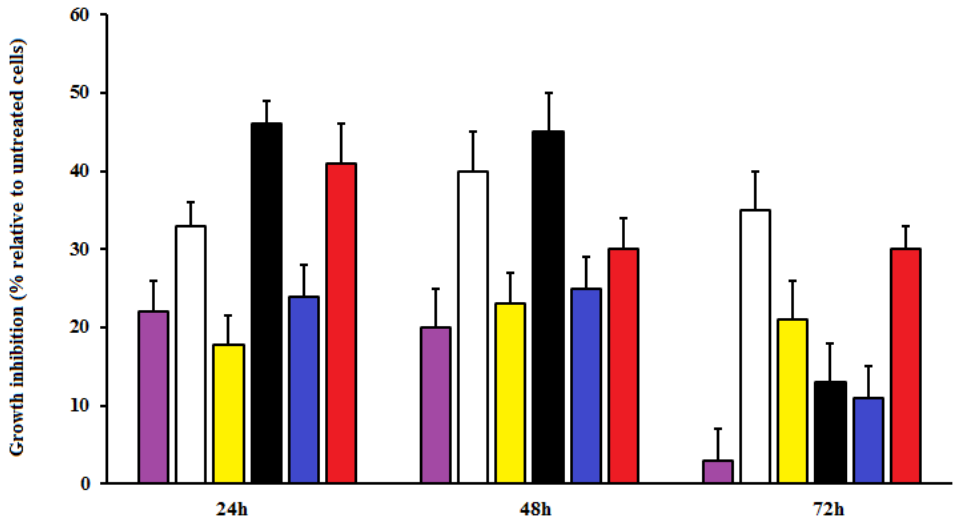

Figure 5. Effect of the different compounds on VEGF-mediated EPCs proliferation. EPCs were grown in a serum and growth factor-free medium containing 20 ng/mL VEGF-A. Cells were exposed to 1μM concentration of different compounds every 24 h (compound **8**, sunitinib; compound **8**+sunitinib, compound **1**, compound **2**, compound **3**). After 24 h, 48 h, and 72 h incubation, cells were counted and cell viability was assessed. Representative of three independent experiments.

Inhibition of TKI activity by conjugates 1-3. To evaluate whether conjugation within **1-3** would affect the TKI activity of the sunitinib-like portion toward its targeted kinases, we firstly evaluated the inhibitory activity of representative compound **3** against human recombinant PDGFRβ and VEGFR2. As shown in Table 4, IC_{50} values were in the nanomolar range, slightly superior than those reported for sunitinib,[13] demonstrating that appendage of the two RGD moieties and linker was not detrimental for TKI activity in vitro.

Table 4. Inhibition of TKI Activity for Compound 3 and the Reference Compound Sunitinib against Human Recombinant PDGFRβ and VEGFR2[a]

Compound	PDGFRβ (nM)	VEGFR2 (nM)
3	9	420
sunitinib	2[b]	80[b]

[a]IC_{50} values for **3** were calculated as the concentration of compound required for 50% inhibition of control specific activity (staurosporine). Each data point represents the average of duplicate wells; data analysis was carried out by nonlinear regression analysis using software developed at Cerep (Hill software). [b]Ref. 13.

The ability of compounds **1**-**3** to inhibit VEGF-stimulated VEGFR2 phosphorylation was investigated by Western blotting using EPCs, which were proven to express high levels of VEGFR2 (besides $\alpha_v\beta_3$). Sunitinib alone, c(AmpRGD) **8** alone, and a combination of the two were also assayed for comparison purposes. Percent inhibition at 1 μM concentration is reported in the densitometric analysis histogram (Figure 6). EPCs were treated for 1 h with the different compounds and then activated with 50 ng/mL VEGF-A for 5min[62] before cell lysis for VEGFR2 phosphorylation detection. Among the different compounds, **1**, **2** and **8** showed a weak induction of VEGFR2 phosphorylation that might be the result of the synergistic intracellular interaction between $\alpha_v\beta_3$ and VEGFR2 probably through Src domains leading to a mild activation of the VEGF receptor.[32,35] As mentioned before, the biological behavior of monomeric compounds **1** and **2** might be influenced more by their RGD moiety rather than the sunitinib moiety, as a consequence of their weak propensity to enter EP cells. Interestingly, dimeric compound **3** induced a marked reduction of VEGFR2 phosphorylation, comparable to that found in EP cells

exposed to sunitinib alone or to the combination of sunitinib + **8**; and this would support the notion that the biological behavior of compound **3** is heavily influenced by its sunitinib moiety, likely due to the enhanced ability to be delivered to the intracellular compartment through the double RGD moieties. Overall, the TKI activity of compound **3** is attributable to the direct interaction with the Y951 domain of VEGFR2 (as sunitinib does) supporting the evidence that **3** acts as genuine VEGFR2 antagonist.

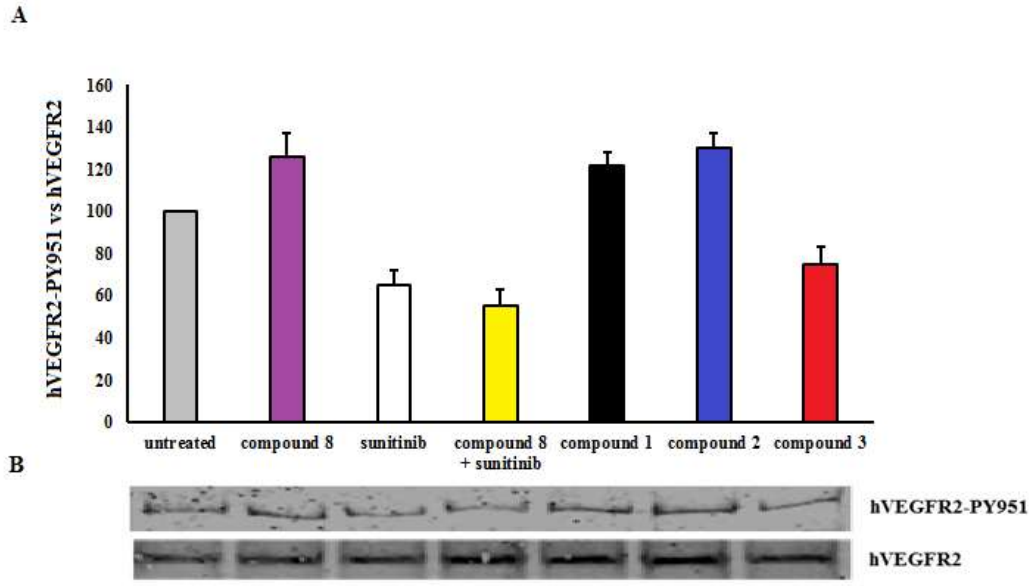

Figure 6. Inhibition of VEGFR2 phosphorylation in EPCs treated for 1 h with 1 μM concentration of different compounds followed by VEGF-A activation (50 ng/mL) for 5 min. A) densitometric analysis of the inhibition of VEGF-induced VEGFR2 phosphorylation; B) western blot analysis. Results are reported as the mean±SD of percent of inhibition of VEGFR phosphorylation compared to VEGF-treated cells. Representative of three independent experiments.

Conjugates 1-3 inhibit the angiogenic process in vitro and in vivo. The ability of conjugates **1-3** to interfere with EP cells in organizing capillary network in vitro was determined. Cells were seeded on Matrigel and exposed to a medium containing VEGF-A (20 ng/mL). Cells were incubated for 6 h in the presence of conjugates **1-3**, unconjugated c(AmpRGD) **8**, sunitinib, and the combination **8**+sunitinib at 0.01, 0.1, and 1.0 μM concentrations. As shown in Figure 7A, a significant or even dramatic reduction in the number of newly formed tubules was observed when EP cells were incubated on Matrigel with the various compounds. The quantification was performed by measuring the number of loops formed by connecting capillary projections (branches) and expressed as percentage of reduction compared to untreated cells, as reported in Figure 7B.

Unconjugated c(AmpRGD) **8** shows a good and dose-related anti-angiogenic activity which is likely due to the inhibitory interaction between the RGD moiety and the extracellular binding domain of $\alpha_V\beta_3$ integrin. Slightly superior anti-angiogenic response is witnessed with sunitinib alone, which clearly owes this behavior to its interaction with the intracellular domain of different kinases, including VEGFR2. Treating EPCs with the combination **8**+sunitinib results in a remarkable dose-dependent (slightly sloped) anti-angiogenic trend, with an exceptional 60% inhibition at 10 nM, much higher than that observed in **8** (19%) and sunitinib (30%) separately. Passing to conjugates **1-3**, the inhibitory activity of angiogenesis is more pronounced for **1** and **3** than for **2**. In particular, for monomeric compound **1** and dimeric derivative **3**, the anti-angiogenesis activity is similar to that of the single **8** or sunitinib at both 1 μM and 0.1 μM concentrations, while it is highly improved (52% for **1** and 43% for **3**) at 10 nM, somehow paralleling the behavior of the combination. This demonstrates that for both the combined and conjugated ingredients, a favorable synergy could exist, given by both the extracellular RGD-

integrin interaction (likely provided by the non-internalized fraction of compounds) and the sunitinib-VEGFR2 kinase interaction (provided by the amount of internalized compound, see also uptake data). Indeed, the partial internalization of the conjugates may be considered a benefit allowing the contemporary action both outside and inside cells.

Overall, the association of the two active modules either in the guise of a combination or as a covalent conjugate is beneficial to gain anti-angiogenic effect in vitro. Which of the two options is better has to be judged after in vivo anti-angiogenesis evaluation, which is able to measure the putative targeting effect within the covalent conjugates.

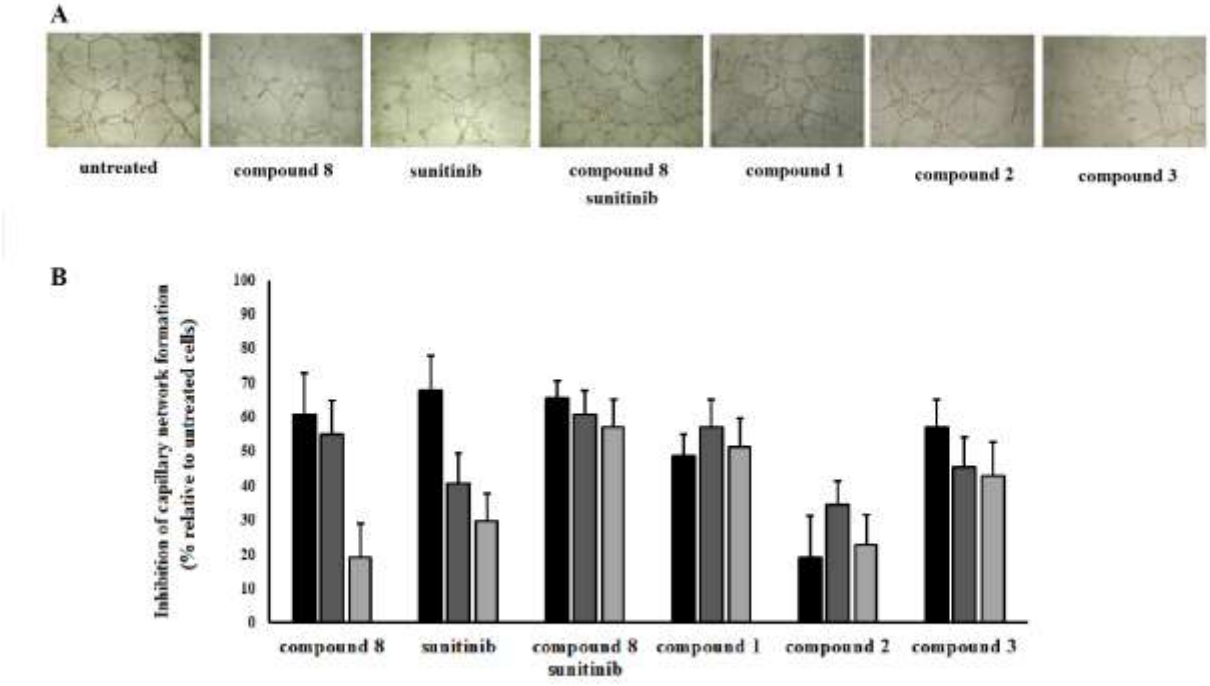

Figure 7. In vitro inhibition of tubulogenesis in VEGF-A activated (20 ng/mL) EPCs seeded on Matrigel and incubated for 6 h with compounds **1**-**3**, c(AmpRGD) **8**, sunitinib, and **8**+sunitinib at 1 μM (black), 0.1 μM (dark grey), and 0.01 μM (grey) concentrations. A) Representative images

of the different treatments at ??? concentration. B) Histograms refer to the inhibition of branches development as compared to untreated cells and expressed as percentage. Representative of three independent experiments??.

We next measured the ability of conjugate **3** (as compared to **8**, sunitinib and their combination) to block angiogenesis in vivo using a Matrigel plug assay. We chose compound **3** for this study as it had the strongest binding to EPCs, it was best internalized, it was the most effective in inhibiting VEGFR2 phosphorylation and capillary tube formation. Despite the very preliminary character of the data obtained, we found that in vivo angiogenesis is scarcely impaired by unconjugated compound **8**, while it is downregulated by sunitinib treatment (Figure 8). This inhibition was comparable to that obtained in the co-treatment, while the injection of compound **3** revealed a consistent reduction of in vivo angiogenesis. These results corroborate the substantial role of conjugate **3** as an anti-angiogenic tool in vivo and substantiate the hypothesis according to which the covalent conjugation of two key angiogenesis-related players (as in **3**) results in a synergic action, even superior to their simple combination.

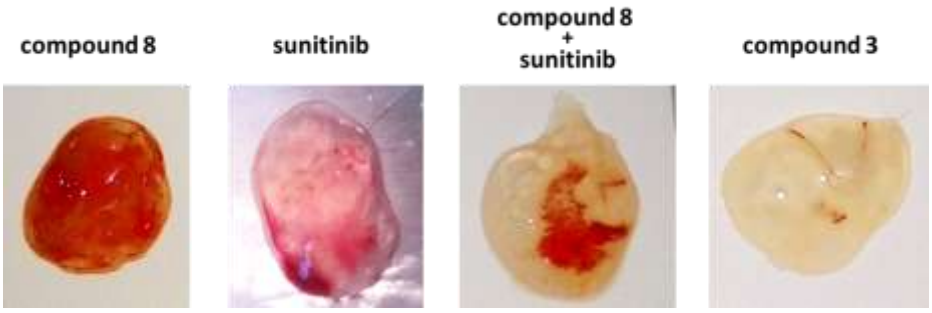

Figure 8. Inhibition of in vivo angiogenesis in Matrigel plugs implanted in FVB mice. Matrigel plugs contained VEGF-A/heparin+10 mg/kg sunitinib or equivalent quantity within **8** or **3**

(compound **8**, sunitinib, sunitinib+**8,** compound **3**). Plugs were removed from mice and photographed after 4 days.

CONCLUSIONS

Three novel molecules, compounds **1**-**3**, were efficiently synthesized and characterized, which featured the robust covalent linkage of a sunitinib-like portion to one or two cyclic aminoproline RGD moieties. Subsequent biological investigations gave important clues about the relative weight of the active modules within the conjugates. Overall, compound **3** seems to best summarize the structural characteristics required for optimal biological response, where both the RGD and the sunitinib modules may exert an active role. The preliminary, relevant anti-angiogenic effect of compound **3** in mice assesses its potential as an effective tool against tumor-associated angiogenesis and is even superior than the simple combination of the two discrete modules. This work stands as a proof-of-concept of how anti-angiogenic small molecules may be selectively delivered to cells through simple, super-targeted anti-angiogenic conjugated molecules to be used in tumor-related or angiogenesis-related therapy.

EXPERIMENTAL SECTION

Chemistry. *General.* All chemicals were of the highest commercially available quality and were used without further purification. Solvents were dried by standard procedures and reactions requiring anhydrous conditions were performed under nitrogen or argon atmosphere. H-Gly-2-ClTrt resin (loading 0.63 mmol/g) was purchased from Novabiochem, (2*S*,4*S*)-Fmoc-4-amino-1-

Boc-pyrrolidine-2-carboxylic acid (**4**) from PolyPeptide and all other reagents from Alfa Aesar, TCI, or Sigma-Aldrich. Flash column chromatography was performed using 40-63 μm silica gel using the indicated solvent mixtures. Automated flash column chromatography was carried out with the Biotage Isolera One system using Biotage KP-Sil cartridges (direct phase) or KP-C18-HS (reverse phase). Melting points (mp) were measured with an optical Optiphot2-Pol thermo-microscope and are uncorrected. Optical rotations were measured using a Perkin-Elmer model 341 polarimeter at ambient temperature using a 100 mm cell with a 1 mL capacity and are given in units of 10^{-1} deg cm^2 g^{-1}. ESI-mass spectra were recorded on API 150EX apparatus and are reported in the form of (*m/z*). HPLC purifications were performed on a Prostar 210 apparatus (Varian, UV detection) equipped with C_{18}-10 μm columns (Discovery BIO Wide Pore 10 × 250 mm or 21.2 × 250 mm). Routine NMR spectra were recorded on Avance 300 or 400 (Bruker) NMR spectrometers. Chemical shifts (δ) are reported in parts per million (ppm) with TMS ($CDCl_3$), CD_2HOD, and HOD resonance peaks set at 0, 3.31, and 4.80 ppm, respectively. Multiplicities are indicated as s (singlet), d (doublet), t (triplet), q (quartet), m (multiplet), and b (broad). Coupling constants, *J*, are reported in Hertz. ^1H and ^{13}C NMR assignments are corroborated by 1D and 2D experiments (gCOSY and gHSQC sequences). High resolution mass analysis (ESI) was performed on LTQ ORBITRAP XL Thermo apparatus. Purity of all tested compounds was determined by analytical high-pressure liquid chromatography (HPLC) and was in the 96 - >99% range.

Materials. H-Gly-2-ClTrt resin (loading 0.63 mmol/g), (2*S*,4*S*)-Fmoc-4-amino-1-Boc-pyrrolidine-2-carboxylic acid (**4**), Fmoc-Asp(*t*Bu)-OH; Fmoc-Arg(Pmc)-OH, 2,4,6-collidine, piperidine, glacial acetic acid, 4-pentynoic acid, 5-fluoroisatin, ethyl 5-formyl-2,4-dimethylpyrrole-3-carboxylate, triethylene glycol, *N*-Boc-ethylenediamine, propargyl bromide,

acetaldehyde, 2-[2-(2-aminoethoxy)ethoxy]ethanol, 3,5-dihydroxybenzoic acid were commercially available and were used as such without further purification. Sunitinib malate salt was purchased by LC Laboratories (USA) with a purity of >99%.

*Synthesis of the c(AmpRGD) Azide **7**.* To a solution of linear tetrapeptide **6** (137 mg, 0.16 mmol, 1 equiv) in dry DCM (35 mL), 2,4,6-collidine (52 µL, 0.39 mmol, 2.5 equiv) was added. The mixture was stirred under argon at room temperature, and added dropwise to a solution of HATU (119 mg, 0.31 mmol, 2 equiv) and HOAt (43 mg, 0.31 mmol, 2 equiv) in dry DMF (5mL) and dry DCM (30 mL). The reaction mixture was degassed by argon/vacuum cycles (3 ×) and left to stir under argon at room temperature for 5 h. After completion, the solution was concentrated under vacuum, treated with aq $NaHCO_3$ saturated solution and extracted with EtOAc (4 ×). The combined organic layers were dried with $MgSO_4$, filtered and evaporated under reduced pressure, keeping the temperature under 50 °C. The crude was purified by reverse phase flash chromatography [H_2O (0.1% TFA)/MeCN: linear gradient 80:20 to 20:80] furnishing the protected c(AmpRGD)-N_3 **7** (90 mg, yield 67%) as a white solid; mp 118.6 °C; $[\alpha]_D^{25}$ = + 19.2 (*c* 0.5; MeOH). ^{1}H NMR (400 MHz, MeOD) δ 4.64 (dd, *J* = 6.3, 5.6 Hz, 1H, Hα Asp), 4.44 (ddd, *J* = 6.9, 6.9, 2.0 Hz, 1H, H4), 4.16 (d, *J* = 13.9 Hz, 1H, Hα Gly), 4.08 (t, *J* = 7.5 Hz, 1H, Hα Arg), 3.64 (d, *J* = 9.2 Hz, 1H, H2), 3.34 (d, *J* = 13.9 Hz, 1H, Hα Gly), 3.30 (t, *J* = 6.6 Hz, 2H, Hδ Arg), 3.27-3.13 (m, 3H, H1′a,b + H5a), 3.04 (bd, *J* = 9.6 Hz, 1H, H5b), 2.76-2.63 (m, 6H, Hβ Asp + CH_2 Pmc + H4′a,b), 2.59 (s, 3H, CH_3 Pmc), 2.57 (s, 3H, CH_3 Pmc), 2.41 (ddd, *J* = 13.6, 9.5, 7.1 Hz, 1H, H3a), 2.12 (s, 3H, CH_3 Pmc), 1.99 (d, *J* = 13.6 Hz ,1H, H3b), 1.86 (t, 2H, CH_2 Pmc), 1.74-1.69 (m, 2H, Hβ Arg), 1.65-1.62 (m, 6H, Hγ Arg + H2′ + H3′), 1.46 (s, 9H, *t*Bu), 1.33 (s, 6H, CH_3 Pmc). ^{13}C NMR (75 MHz, MeOD) δ 177.3 (Cq), 175.4 (Cq), 170.6 (Cq), 170.1 (Cq), 169.8 (Cq), 156.8 (Cq), 153.5 (Cq),

138.5 (Cq), 135.3 (Cq), 134.9 (Cq), 133.5 (Cq), 123.8 (Cq), 118.2 (Cq), 81.0 (Cq), 73.7 (CH_2), 62.7 (CH_2), 60.0 (CH_2), 55.1 (CH), 52.3 (CH_2), 51.0 (CH_2), 49.8 (CH), 49.1 (CH), 44.4 (CH_2), 40.1 (CH), 37.3 (CH_2), 36.1 (CH_2), 32.6 (CH_2), 27.1 (3C, CH_3), 26.9 (CH_2), 26.5 (CH_2), 25.8 (2C, CH_3), 25.7 (CH_2), 21.2 (CH_2), 17.8 (CH_3), 16.7 (CH_3), 11.1 (CH_3). HRMS (ES^+) $C_{39}H_{61}N_{11}O_9S$ calcd for $[M+H]^+$ 860.4447, found 860.4470.

*Synthesis of the c(AmpRGD) Amine **8**.* The cyclic tetrapeptide **7** (29 mg, 0.03 mmol) was dissolved in EtOH (4 mL) and a catalytic amount of 10% palladium on carbon was added. The reaction vessel was degassed under vacuum and thoroughly purged with hydrogen (3 ×). The resulting heterogeneous mixture was stirred overnight under hydrogen at room temperature, then the catalyst was filtered off and the filtrate was concentrated under vacuum. The protected intermediate AmpRGD-NH_2 (27 mg, 0.03 mmol) was dissolved in 1.6 mL of a TFA/TIS/H_2O (95:2.5:2.5) mixture and stirred at room temperature for 2.5 h. Then, the solvent was evaporated and the crude residue was thoroughly washed with Et_2O (4 ×) and petroleum ether (2 ×). Preparative RP-HPLC purification was performed [C_{18}-10 μm column, 21.2 × 250 mm; solvent A: H_2O (0.1% TFA) and solvent B: MeCN, flow rate 8 mL/min; detection 220 nm] using a linear gradient from 100% A to 25% B in 25 min. The removal of the solvent under vacuum, keeping the temperature under 50 °C, furnished c(AmpRGD)-NH_2 **8** (18.4 mg, TFA salt, yield 91%) as a colourless glassy solid; $[\alpha]_D^{25}$ = –13.3 (*c* 1.0, H_2O). ^{1}H NMR (400 MHz, D_2O) δ 4.60 (dd, *J* = 6.2, 6.2 Hz, 1H, Hα Asp), 4.52 (d, *J* = 10.8 Hz, 1H, H2), 4.26 (bt, *J* = 4.9 Hz, 1H, H4), 4.12 (dd, *J* = 7.5, 7.5 Hz, 1H, Hα Arg), 3.94 (d, *J* = 13.9 Hz, 1H, Hα Gly), 3.93 (m, 1H, H5a), 3.37 (bd, *J* = 8.8 Hz, 1H, H5b), 3.21 (m, 2H, H4′), 3.09 (t, *J* = 6.8 Hz, 2H, Hδ Arg), 2.90–2.81 (m, 3H, H1′ + H3a), 2.80 (d, *J* = 5.9 Hz, 2H, Hβ Asp), 2.42 (bd, *J* = 15.2 Hz, 1H, H3b), 1.68–1.46 (m, 8H, Hβ Arg + Hγ Arg + H2′ + H3′). ^{13}C NMR (100 MHz, D_2O) δ 176.2 (Cq), 174.5 (Cq), 172.7 (Cq),

171.2 (2C, Cq), 156.9 (Cq), 66.0 (CH), 60.2 (CH_2), 56.1 (CH), 49.9 (CH), 44.6 (CH_2), 40.6 (CH_2), 38.8 (CH_2), 35.1 (CH_2), 35.0 (CH_2), 34.9 (CH_2), 26.5 (CH_2), 24.6 (CH_2), 23.8 (CH_2), 22.3 (CH_2). HRMS (ES^+) $C_{21}H_{37}N_9O_6$ calcd for $[M+H]^+$ 512.2940, found 512.2932.

*Synthesis of compound **15**.* To a solution of **13** (94 mg, 0.31 mmol, 1 equiv) in dry DCM (1.5 mL) and dry DMF (2.5 mL), BOP (70 mg, 0.16 mmol, 1.3 equiv) and DIPEA (85 µL, 0.49 mmol, 4 equiv) were added and, after 5 min, a solution of **14** (103 mg, 0.41 mmol, 1.3 equiv) in dry DCM (1.5 mL) and dry DMF (1 mL) was added. The reaction was stirred under argon at room temperature, protected from light. A yellow precipitate started to form after 1 h. After 5 h the reaction was over and Et_2O (3 mL) and petroleum ether (3 mL) were added to the mixture. The solid was collected by vacuum filtration and washed with H_2O (3 ×) furnishing compound **15** (116 mg, yield 88%) as an orange solid; mp> 220 °C. ^{1}H NMR (400 MHz, DMSO-d_6) δ 13.69 (s, 1H, NH), 10.89 (s, 1H, NH), 8.02 (bt, J = 4.5 Hz, 1H, NH), 7.76 (dd, J = 9.5, 2.0 Hz, 1H, H4), 7.72 (s, 1H, H1′), 7.60 (bt, J = 5.0 Hz, 1H, NH), 6.92 (ddd, J = 8.8, 8.8, 2.0 Hz, 1H, H6), 6.85 (dd, J = 9.2, 4.4 Hz, 1H, H7), 3.28 (m, 2H, CH_2), 3.24 (m, 2H, CH_2), 2.76 (t, J = 2.4 Hz, ≡CH), 2.44 (s, 3H, CH_3), 2.42 (s, 3H, CH_3), 2.37 (m, 2H, CH_2), 2.29 (t, J = 7.1 Hz, 2H, CH_2). ^{13}C NMR (100 MHz, DMSO-d_6) δ 171.1 (Cq), 170.0 (Cq), 165.4 (Cq), 158.6 (d, $^1J_{CF}$ = 233 Hz, Cq), 137.1 (Cq), 135.0 (Cq), 130.8 (Cq), 127.6 (d, $^3J_{CF}$ = 10 Hz, Cq), 126.3 (CH), 125.3 (Cq), 121.0 (Cq), 115.1 (Cq), 112.8 (d, $^2J_{CF}$ = 25 Hz, CH), 110.4 (d, $^3J_{CF}$ = 8 Hz, CH), 106.3 (d, $^2J_{CF}$ = 26 Hz, CH), 84.2 (Cq), 71.7 (CH), 46.6 (CH_2), 34.8 (CH_2), 19.3 (CH_2), 14.7 (CH_2), 13.8 (CH_3), 11.0 (CH_3). HRMS (ES^+) $C_{23}H_{23}FN_4O_3$ calcd for $[M+H]^+$ 423,1827, found 423,1823.

*Synthesis of compound **17**.* To a stirred suspension of **13** (11mg, 0.04 mmol, 1 equiv) in dry DMF (500 µL), BOP (21 mg, 0.05 mmol, 1.3 equiv) and DIPEA (26 µL, 0.15 mmol, 4 equiv) were added and, after 5 min, a solution of **16** (15 mg, 0.04 mmol, 1.1 equiv) in dry DCM (400

µL) was added. The reaction mixture was stirred under argon at room temperature for 3 h protected from light. After reaction completion, the solvent was evaporated under reduced pressure, the residue was washed with water (3 ×), and the solvent was removed by a Pasteur pipette. The yellow-orange crude was purified by silica gel flash chromatography [gradient elution from 100% EtOAc to 90:10 EtOAc/MeOH(NH_3)] affording **17** (12.7 mg, yield 64%) as a yellow-orange glassy solid. ^{1}H NMR (400 MHz, MeOD) δ 7.58 (s, 1H, =CH), 7.45-7.39 (m, 1H, ArH), 6.90–6.83 (m, 2H, ArH), 4.14 (d, ^4J = 2.4 Hz, 2H, -O*CH*$_2$C≡CH), 3.65–3.53 (m, 10H, -OCH_2), 3.50 (t, J = 6.5 Hz, 2H, -CONH*CH*$_2$), 2.81 (t, ^4J = 2.4 Hz, 1H, ≡CH), 2.81–2.76 (bm, 4H, -NCH_2), 2.72 (q, J = 7.1 Hz, 2H, -NC*H*$_2$$CH_3$), 2.52 (s, 3H, CH_3), 2.49 (s, 3H, CH_3), 1.12 (t, J = 7.1 Hz, 3H, CH_3). ^{13}C NMR (75 MHz, MeOD) δ 171.8 (Cq), 168.5 (Cq), 160.6 (d, $^1J_{CF}$ = 236 Hz, Cq), 138.3 (Cq), 136.0 (Cq), 131.7 (Cq), 128.8 (d, $^3J_{CF}$ = 9 Hz, Cq), 127.6 (Cq), 125.5 (CH), 121.2 (Cq), 116.9 (Cq), 113.9 (d, $^2J_{CF}$ = 25 Hz, CH), 111.3 (d, $^3J_{CF}$ = 8 Hz, CH), 106.5 (d, $^2J_{CF}$ = 26 Hz, CH), 80.7 (Cq), 76.1 (CH), 71.6 (CH_2), 71.5 (2C, CH_2), 71.5 (CH_2), 70.8 (CH_2), 70.2 (CH_2), 59.1 (CH_2), 54.0 (CH_2), 53.9 (CH_2), 49.7 (CH_2), 38.5 (CH_2), 13.7 (CH_3), 12.2 (CH_3), 11.1 (CH_3). HRMS (ES^+) $C_{29}H_{37}FN_4O_5$ calcd for $[M+H]^+$ 541.2821, found 541.2817.

*Synthesis of compound **19**.* To a stirred suspension of **13** (7.7 mg, 0.026 mmol, 1.2 equiv) in dry DMF (200 µL), BOP (13.3 mg, 0.03 mmol, 1.4 equiv) and DIPEA (15 µL, 0.09 mmol, 4 equiv) were added and, after 5 min, a solution of **18** (11.7 mg, 0.21 mmol, 1 equiv) in dry DCM (200 µL) and dry DMF (100 µL) was added. The reaction mixture was left to stir under argon at room temperature for 16 h, protected from light. After reaction completion, the solvent was evaporated under reduced pressure and the residue was re-dissolved in EtOAc (2 mL) and the solution was washed with H_2O (2 ×) and saturated aqueous $NaHCO_3$ solution (2 ×). The organic layer was collected and concentrated under vacuum, affording an orange crude residue which was purified

by silica gel flash chromatography [EtOAc/MeOH(NH_3), 95:5] affording compound **19** (10.2 mg, yield 67%) as yellow glassy solid. ^{1}H NMR (400 MHz, MeOD) δ 7.47 (bs, 1H, =CH), 7.35 (m, 1H, H4 suni), 7.05 (d, ^4J = 2.3 Hz, 2H, ArH), 6.86–6.80 (m, 2H, H6, H7 suni), 6.75 (t, J = 2.3 Hz, 1H, ArH), 4.74 (d, ^4J = 2.3 Hz, 4H, ArOCH_2), 3.63–3.57 (m, 8H, -OCH_2), 3.52–3.44 (m, 4H, -CONHCH_2), 2.99 (t, ^4J = 2.3 Hz, 2H, -≡CH), 2.77–2.69 (m, 6H, -NCH_2), 2.48 (s, 3H, CH_3), 2.43 (s, 3H, CH_3), 1.08 (t, ^3J = 7.1 Hz, 3H, -NCH_2CH_3). ^{13}C NMR (100 MHz, MeOD) δ 170.1 (Cq), 168.0 (Cq), 166.9 (Cq), 159.0 (d, $^1J_{CF}$ = 236.5 Hz, Cq), 158.8 (2C, Cq), 136.7 (Cq), 136.2 (Cq), 134.4 (Cq), 130.0 (Cq), 127.3 (d, $^3J_{CF}$ = 9 Hz, Cq), 126.1 (Cq), 123.8 (CH), 119.5 (Cq), 115.3 (d, $^4J_{CF}$ = 2.9 Hz, Cq), 112.3 (d, $^2J_{CF}$ = 24.3 Hz, CH), 109.8 (d, $^3J_{CF}$ = 8.5 Hz, CH), 106.6 (2C, CH), 104.9 (d, $^2J_{CF}$ = 27.3 Hz, CH), 104.8 (CH), 78.0 (2C, Cq), 75.8 (2C, CH), 70.0 (CH_2), 69.9 (CH_2), 69.1 (CH_2), 69.0 (CH_2), 55.6 (2C, CH_2), 52.4 (2C, CH_2), 48.1 (CH_2), 39.5 (CH_2), 36.9 (CH_2), 12.2 (CH_3), 10.6 (CH_3), 9.6 (CH_3). HRMS (ES^+) $C_{39}H_{44}FN_5O_7$ calcd for $[M+H]^+$ 714.3298, found 714.3290.

*Synthesis of the Sunitinib-c(AmpRGD) Conjugate **1**.* A stirred solution of compounds **7** (20 mg, 0.02 mmol, 1 equiv) and **15** (12.8 mg, 0.03 mmol, 1.3 equiv) in dry DMF (2 mL) was degassed at room temperature by argon/vacuum cycles (3 ×). To this solution was added a freshly prepared aqueous mixture (1 mL) of $Cu(OAc)_2$ (1.39 mg, 0.007 mmol, 0.3 equiv) and sodium ascorbate (2.8 mg, 0.014 mmol, 0.6 equiv), previously degassed by argon/vacuum cycles (3 ×). The reaction mixture was degassed again and left to stir, protected from light, under argon at room temperature for 20 h. After reaction completion, the mixture was concentrated under vacuum, keeping the temperature under 50 °C. The crude was dissolved with 5 drops of MeOH, and a yellow precipitate adhering to the round-bottom flask walls was obtained by means of the dropwise addition of Et_2O and petroleum ether. The organic solvents were removed by a Pasteur

pipette. Subsequently, the residue was treated with water (3 ×), and the solvent was removed by a Pasteur pipette, affording a yellow-orange solid, which was used in the following step without further purification. The crude intermediate (30 mg, 0.02 mmol) was treated with a solution (1.2 mL) of TFA/TIS/H_2O (95:2.5:2.5) and the reaction mixture was left to stir for 2 h under argon at room temperature, protected from light. After solvent evaporation, the crude residue was washed thoroughly with Et_2O (4 ×) and petroleum ether (2 ×). Preparative RP-HPLC purification was performed [C_{18}-10 µm column, 21.2 × 250 mm; solvent A: H_2O (0.1% TFA) and solvent B: MeCN; flow rate 8.0 mL/min; detection 421 nm] using the following gradient elution: 0-1 min 5% B, 1-20 min 5-35% B, 20-28 min 35% B; R_t = 26.9 min. Product **1** (17.3 mg, yield 69%) was obtained as an orange glassy solid. $[\alpha]_D^{25}$ = – 7.70 (*c* 1.0; MeOH). ^{1}H NMR (400 MHz, MeOD) δ 7.77 (s, 1H, ArH), 7.55 (s, 1H, =CH), 7.40 (m, 1H, ArH), 6.87 (m, 2H, ArH), 4.72 (t, *J* = 5.9 Hz, 1H, Hα Asp), 4.53 (d, *J* = 11 Hz, 1H, H2 Amp), 4.38 (t, *J* = 6.4 Hz, 2H, H1′), 4.31 (bm, 1H, H4 Amp), 4.25 (t, *J* = 7.3 Hz, 1H, Hα Arg), 4.08 (d, *J* = 13.6 Hz, 1H, Hαa Gly), 4.03 (m, 1H, H5a Amp), 3.50 (m, 2H, H1′′′), 3.47–3.40 (m, 3H, H2′′′ + H5b Amp), 3.41 (d, *J* = 13.6 Hz, 1H, Hαb Gly), 3.31–3.20 (m, 4H, Hδ Arg + H4′), 3.03 (t, *J* = 7.2 Hz, 2H, H2′′), 2.90 (m, 1H, H3a Amp), 2.84 (d, *J* = 5.8 Hz, 2H, Hβ Asp), 2.71–2.56 (m, 3H, H3b Amp + H1′′), 2.48 (s, 3H, CH_3), 2.44 (s, 3H, CH_3), 2.02–1.86 (m, 2H, H2′), 1.86–1.48 (m, 6H, Hβ Arg + H3′ + Hγ Arg). ^{13}C NMR (100 MHz, MeOD) δ 175.6 (Cq), 173.7 (Cq), 172.9 (Cq), 171.8 (Cq), 170.9 (Cq), 170.1 (Cq), 170.0 (Cq), 167.3 (Cq), 159.0 (d, $^1J_{CF}$ = 236 Hz, Cq), 157.3 (Cq), 146.6 (Cq), 136.7 (Cq), 134.4 (Cq), 130.1 (Cq), 127.2 (d, $^3J_{CF}$ = 9 Hz, Cq), 126.1 (Cq), 123.7 (CH), 122.3 (CH), 119.4 (Cq), 115.3 (Cq), 112.3 (d, $^2J_{CF}$ = 25 Hz, CH), 109.8 (d, $^3J_{CF}$ = 8 Hz, CH), 104.8 (d, $^2J_{CF}$ = 26 Hz, CH), 65,9 (CH), 60.3 (CH_2), 55.8 (CH), 54.6 (CH_2), 50.0 (CH), 49.7 (CH), 48.8 (CH_2), 44.5 (CH_2), 40.5 (CH_2), 39.0 (CH_2), 38.9 (CH_2), 34.9 (CH_2), 34.8 (CH_2), 34.7 (CH_2), 26.9 (CH_2), 26.5

(CH_2), 25.2 (CH_2), 22.3 (CH_2), 21.1 (CH_2), 12.1 (CH_3), 9.5 (CH_3). HRMS (ES$^+$) $C_{44}H_{58}FN_{15}O_9$ calcd for $[M+H]^+$ 960.4599, found 960.4576.

*Synthesis of the Sunitinib-c(AmpRGD) Conjugate **2**.* Compound **2** was prepared according to the procedure described for the synthesis of compound **1**, starting from **7** (6.5 mg, 0.0076 mmol, 1 equiv) and **17** (5.3 mg, 0.0098 mmol, 1.3 equiv) in dry DMF (700 µL) and using $Cu(OAc)_2$ (0.45 mg, 0.002 mmol, 0.3 equiv), sodium ascorbate (0.9 mg, 0.0045 mmol, 0.6 equiv) in H_2O (300 µL). After 24 h, the protected intermediate (9 mg, 0.006 mmol) was treated with a solution of TFA/TIS/H_2O (321 µL). Preparative RP-HPLC purification was performed [C_{18}-10 µm column, 21.2 × 250 mm; solvent A: H_2O (0.1% TFA) and solvent B: MeCN, flow rate 8.0 mL/min; detection 421 nm] using the following gradient elution: 0-1 min 5% B, 1-20 min 5-35% B, 20-28 min 35% B; R_t = 26.4 min. Conjugate **2** (6.3 mg, as TFA salt, yield 70% for two steps) was obtained as yellow-orange glassy solid. $[\alpha]_D^{20}$ = – 8.75 (*c* 0.16; MeOD). ^{1}H NMR (400 MHz, MeOD) δ 7.96 (s, 1H, CH triazole), 7.63 (s, 1H, =CH),7.49–7.45 (m, 1H, ArH), 6.93–6.88 (m, 2H, ArH), 4.72 (t, *J* = 6.0 Hz, 1H, Hα Asp), 4.60 (s, 2H, -OC*H*$_2$-triazole), 4.56 (bd, *J* = 11 Hz, 1H, H2 Amp), 4.43 (t, *J* = 6.0 Hz, 2H, H1′), 4.30 (m, 1H, H4 Amp), 4.24 (t, *J* = 7.2 Hz, 1H, Hα Arg), 4.11–4.00 (bm, 2H, Hαa Gly, H5a Amp), 3.93–3.88 (m, 2H, -OCH_2), 3.80–3.73 (m, 2H, -CONHC*H*$_2$), 3.71–3.62 (m, 8H, -OCH_2), 3.55–3.36 (bm, 8H, -NCH_2, Hαb Gly, H5b Amp), 3.31–3.22 (bm, 4H, Hδ Arg, H4′), 2.97–2.82 (bm, 3H, H3a Amp, Hβ Asp), 2.68 (bd, *J* = 14.4 Hz, 1H, H3b Amp), 2.55 (s, 3H, CH_3), 2.51 (s, 3H, CH_3), 2.01–1.91 (bm, 2H, H2′), 1.86–1.58 (bm, 6H, Hβ Arg, H3′, Hγ Arg), 1.41 (t, *J* = 7.2 Hz, 3H, CH_3). ^{13}C NMR (100 MHz, MeOD) δ 175.7 (Cq), 172.8 (Cq), 171.8 (Cq), 170.9 (Cq), 170.3 (Cq), 170.1 (Cq), 168.7 (Cq), 159.1 (d, $^1J_{CF}$ = 236 Hz, Cq), 157.3 (Cq), 146.5 (Cq), 137.4 (Cq), 134.6 (Cq), 130.2 (Cq), 127.1 (d, $^3J_{CF}$ = 9 Hz, Cq), 126.2 (Cq), 123.8 (2C, CH), 118.1 (Cq), 116.1 (Cq), 112.7 (d, $^2J_{CF}$ = 25 Hz, CH), 110.0 (d, $^3J_{CF}$

= 9 Hz, CH), 105.2 (d, $^{2}J_{CF}$ = 26 Hz, CH), 70.0 (2C, CH_2), 69.4 (2C, CH_2), 66.1 (CH), 64.3 (CH_2), 63.5 (CH_2), 60.2 (CH_2), 55.9 (CH), 54.7 (CH_2), 53.6 (CH_2), 52.7 (CH_2), 50.1 (CH), 49.7 (CH), 49.2 (CH_2), 48.9 (CH_2), 44.5 (CH_2), 40.5 (CH_2), 35.2 (CH_2), 34.7 (CH_2), 34.0 (CH_2), 26.9 (CH_2), 26.6 (CH_2), 25.2 (CH_2), 22.4 (CH_2), 12.4 (CH_3), 9.6 (CH_3), 7.9 (CH_3). HRMS (ES^+) $C_{50}H_{72}FN_{15}O_{11}$ calcd for $[M+H]^+$ 1078.5593, found 1078.5585.

*Synthesis of the Sunitinib-c(AmpRGD) Conjugate **3**.* Compound **3** was prepared according to the procedure described for the synthesis of compound **1**, starting from **7** (28.1 mg, 0.033 mmol, 2.3 equiv) and **19** (10.2 mg, 0.014 mmol, 1 equiv) in dry DMF (2 mL) and using $Cu(OAc)_2$ (1.7 mg, 0.01 mmol, 0.6 equiv), sodium ascorbate (3.4 mg, 0.02 mmol, 1.2 equiv) in H_2O (0.9 mL). After 24 h, the protected intermediate (32.3 mg, 0.013 mmol) was treated with a solution of TFA/TIS/H_2O (321 µL). Preparative RP-HPLC purification was performed [C_{18}-10 µm column, 21.2 × 250 mm; solvent A: H_2O (0.1% TFA) and solvent B: MeCN, flow rate 8.0 mL/min; detection 421 nm] using the following gradient elution: 0-1 min 5% B, 1-23 min 5-40% B, 23-28 min 40% B; R_t = 21.8 min. Conjugate **3** (12.4 mg, as TFA salt, yield 43%) was obtained as a yellow glassy solid. $[\alpha]_D^{20}$ = – 6.92 (*c* 0.39; MeOH). ^{1}H NMR (400 MHz, MeOD) δ 8.06 (s, 2H, =CH triazole), 7.54 (s, 1H, =CH), 7.41 (m, 1H, H4 suni), 7.07 (d, ^{4}J = 2.0 Hz, 2H, ArH), 6.91–6.86 (m, 2H, H6 + H7 suni), 6.70 (bt, ^{4}J = 2.0 Hz, 1H, ArH), 5.21 (d, ^{2}J = 12.2 Hz, 2H, ArOCHa), 5.15 (d, ^{2}J = 12.2 Hz, 2H, ArOCHb), 4.69 (t, *J* = 5.8 Hz, 2H, Hα Asp), 4.59 (bd, *J* = 10.6 Hz, 2H, H2 Amp), 4.51–4.44 (m, 4H, H1′), 4.33 (bs, 2H, H4 Amp), 4.22 (bt, *J* = 6.6 Hz, 2H, Hα Arg), 4.13–4.01 (bm, 4H, Hαa Gly + H5a Amp), 3.93–3.87 (bm, 2H, -OCH_2), 3.79–3.63 (bm, 8H, -CONHCH_2,-OCH_2), 3.60–3.38 (bm, 12H, -CONHCH_2, Hαb Gly, H5b Amp + -NCH_2), 3.31 (bm, 4H, Hδ Arg), 3.26–3.21 (bm, 4H, H4′), 3.00–2.88 (bm, 2H, H3a Amp), 2.88–2.74 (m, 4H, Hβ Asp), 2.73–2.65 (bd, *J* = 14.7 Hz, 2H, H3b Amp), 2.50 (s, 3H, CH_3), 2.46 (s, 3H, CH_3),

2.04–1.92 (bm, 4H, H2′), 1.84–1.57 (bm, 12H, Hβ Arg, H3′, Hγ Arg), 1.39 (t, J = 7.2 Hz, 3H, -NCH_2CH_3). ^{13}C NMR (100 MHz, MeOD) δ 175.6 (Cq), 172.8 (Cq), 171.8 (Cq), 171.0 (Cq), 170.2 (Cq), 169.9 (Cq), 168.7 (Cq), 168.4 (Cq), 159.4 (2C, Cq), 159.1 (d, $^1J_{CF}$ = 236.7 Hz, Cq), 157.3 (2C, Cq), 143.5 (2C, Cq), 137.4 (Cq), 136.4 (Cq), 134.6 (Cq), 130.2 (Cq), 127.2 (d, $^3J_{CF}$ = 9.1 Hz, Cq), 126.2 (Cq), 124.1 (2C, CH), 123.8 (CH), 118.0 (Cq), 115.9 (d, $^4J_{CF}$ = 2.9 Hz, Cq), 112.6 (d, $^2J_{CF}$ = 24.0 Hz, CH), 110.0 (d, $^3J_{CF}$ = 8.3 Hz, CH), 106.3 (2C, CH), 105.1 (d, $^2J_{CF}$ = 26.0 Hz, CH), 104.9 (CH), 70.2 (CH_2), 69.8 (CH_2), 69.1 (CH_2), 65.9 (2C, CH), 64.3 (CH_2), 61.2 (2C, CH_2), 60.5 (2C, CH), 55.9 (2C, CH), 54.6 (2C, CH_2), 52.7 (CH_2), 50.1 (2C, CH), 49.6 (2C, CH), 49.1 (4C, CH_2), 44.6 (2C, CH_2), 40.5 (2C, CH_2), 39.5 (CH_2), 35.3 (CH_2), 34.9 (2C, CH_2), 34.7 (2C, CH_2), 26.9 (2C, CH_2), 26.5 (2C, CH_2), 25.2 (2C, CH_2), 22.4 (2C, CH_2), 12.4 (CH_3), 9.6 (CH_3), 7.9 (CH_3). HRMS (ES^+) $C_{81}H_{114}FN_{27}O_{19}$ calcd for $[M+2H]^{2+}$ 894.9457, found 894.9479.

Biology. All experimental procedures involving animals were performed in accordance with national guidelines, approved by the ethical committee of Animal Welfare Office of Italian Work Ministry (401/2015PR approved 05/21/2015) and conformed to the legal mandates and Italian guidelines for the care and maintenance of laboratory animals.

Cell Lines and Culture Conditions. Endothelial progenitor cells (EPC) were kindly provided by Prof. M. Del Rosso of the Department of Experimental and Clinical Biomedical Science, University of Florence. Human umbilical cord blood (UCB) samples of health newborns were used as a source of EPCs, as previously described.[63] EPCs were cultured on gelatin 1 %-coated dishes in complete endothelial cell growth medium (EGM-2 BulletKit, Lonza), which includes endothelial basal medium plus the SingleQuots Kit (hydrocortisone, human fibroblast growth factor B, VEGF, LongR3 insulin-like growth factor 1, ascorbic acid, human epidermal growth

factor, GA-1000, and heparin), supplemented with antibiotics (100 UI/mL penicillin, 100 lg/mL streptomycin) and 10 % FBS. Cells were used between the third and tenth passages in vitro.

In Vitro Plasma Stability. Plasma was quickly thawed and diluted to 80% (v/v) with 100 mM Phosphate Buffered Saline (PBS) pH 7.4 to control pH over the time period of the experiments. Stock solutions of sunitinib and test compounds were added (final compound concentration: 1 μM) and maintained at 37 °C. At regular time points, aliquots of plasma solution were sampled, two volumes of MeCN were added, samples were centrifuged (9,000 g, 10 min, 4 °C) and analyzed by HPLC-UV-Vis for percentage of remaining compound over incubation time.

Lipophilicity. Distribution coefficients (Log $D_{oct,7.4}$) values in the *n*-octanol/buffer partition system for sunitinib and compounds **1-3** were measured at room temperature (25±3 °C) by the reference shake-flask method. Buffer was 50 mM MOPS (3-morpholinopropanesulfonic acid), pH 7.4, with ionic strength adjusted to 0.15M for KCl addition. Test compounds, after equilibrating for 4 h between pre-saturated partition phases under dark, were analyzed in each phase by HPLC-UV-Vis, after dilution of each partition phase with MeOH. The Log $D_{oct,7.4}$ values reported in Table are the means of at least three partition experiments employing different *n*-octanol/buffer volume ratios.

Cell Uptake. Total intracellular concentrations of **1-3** and sunitinib were determined as previously reported with minor modifications.[64] Briefly, EPCs were seeded in 6-well plates and cultivated to confluence in complete medium. After 24 h, medium was replaced by fresh serum and growth factor-free medium containing test compounds (sunitinib, **1-3**) at 1 μM concentration. EPCs were incubated for 1 h at 37 °C and tested either immediately after or 8 h after removal of the compound from the extracellular medium by washing the cells twice with 1

mL aliquots of PBS. Cell monolayers were next lysed and compounds were then extracted using 1 mL of absolute ethanol/well at 4 °C. Cell extracts were centrifuged (13000 rpm, 5 min, 4 °C) to separate the supernatant which was then dried under nitrogen flow, dissolved in HPLC eluent and injected into the HPLC-ESI-MS/MS system for quantification. Intracellular content of test compounds was quantified as nmol compound/mg protein content in each sample. Cell pellets were solubilized using 0.2 M NaOH for 5 min following the addition of the standard lysis buffer and protein content was determined using the Bradford dye.

For specific displacement experiments, growing EP cells were detached from cultures by gentle treatment with Accutase, washed, and resuspended in a serum-free medium and exposed to conjugated compounds **2** and **3** or sunitinib at 1 μM concentration in the presence or in the absence of compound **8** at 100 μM concentration. Cells were then incubated at 37 °C with 10% CO_2. At the end of incubation, the cell suspensions were washed by centrifugation at 1200 rpm for 5 min at 4 °C. Supernatants were discarded and ethanol extraction of the cell pellets was performed at 4 °C for 10 min. Cell extracts were centrifuged at 14000 rpm for 5 min at 4 °C and supernatants were evaporated under a stream of pure nitrogen for HPLC-ESI-MS/MS quantification, as above.

Cytofluorimetric assay. Cells were detached by gentle treatment with Accutase (Lonza), a 0.5 mm EDTA solution, washed, and incubated for 1 h at 4 °C in the presence of anti-$\alpha_V\beta_3$ monoclonal antibody (1 μg/50 μL, anti-integrin $\alpha_V\beta_3$, clone LM609, Millipore). Cells were then washed and incubated for 1 h at 4 °C with a specific secondary antibody, 5 mg/Ml 1 μL/50 μL goat antimouse IgG conjugated with fluorescein isothiocyanate (FITC; Santa Cruz Biotecnology,

Inc., SantaCruz, CA). Integrin-positive cells were analyzed at 488 nm using a FACScan system flow cytometer (BD-FACS Canto).

Solid-phase receptor binding assay. Recombinant human integrin $\alpha_V\beta_3$ and $\alpha_5\beta_1$ receptors (R&D Systems, Minneapolis, MN, USA) were diluted to 0.5 μg/mL in coating buffer containing 20 mM Tris-HCl (pH 7.4), 150 mM NaCl, 1 mM $MnCl_2$, 2 mM $CaCl_2$, and 1 mM $MgCl_2$. An aliquot of diluted receptor (100 μL/well) was added to 96-well microtiter plates and incubated overnight at 4 °C. The plates were incubated with blocking solution (coating buffer plus 1% bovine serum albumin) for additional 2 h at room temperature to block nonspecific binding. After washing 2 times with blocking solution, plates were incubated 3 h at room temperature, in the dark, with various concentrations (10^{-5}–10^{-12} M) of test compounds in the presence of 1 μg/mL biotinylated vitronectin (for integrin $\alpha_V\beta_3$, vitronectin purchased from Molecular Innovations, Novi, MI, USA) or biotinylated fibronectin (for integrin $\alpha_5\beta_1$, fibronectin purchased from Sigma). Biotinylation was performed using an EZ-Link Sulfo-NHS-Biotinylation kit (Pierce, Rockford, IL, USA). After washing 3 times, the plates were incubated for 1 h at room temperature with streptavidin-biotinylated peroxidase complex (Amersham Biosciences, Uppsala, Sweden). Plates were washed 3 times with blocking solution, followed by 30 min incubation with 100 μL/well Substrate Reagent Solution (R&D Systems, Minneapolis, MN, USA) before stopping the reaction with the addition of 50 μL/well 2N H_2SO_4. Absorbance at 415 nm was read in a SynergyTM HT Multi-Detection Microplate Reader (BioTek Instruments, Inc.). Each data point represents the average of triplicate wells; data analysis was carried out by nonlinear regression analysis with GraphPad Prism software. Each experiment was repeated in duplicate.

Cell-adhesion assay. Plates (96 wells) were coated with vitronectin (10 mg/mL) by overnight incubation at 4 °C. Plates were washed with phosphate buffer solution (PBS) and then incubated at 37 °C for 1 h with PBS/1% BSA. After being washed, EPCs were counted and resuspended in serum-free medium, then exposed to the compound (final concentration was 1, 10, 100, 1000, 10000 nM) at 37 °C for 30 min to allow the ligand–receptor equilibrium to be reached. Assays were performed in the presence of 2.0 mmol/L $MnCl_2$. Cells were then plated (5-6×10^4cells per well) and incubated at 37 °C for 1 h. All the wells were washed with PBS to remove the non-adherent cells, and 0.5% crystal violet solution in 20% methanol was added. After 2 h of incubation at 4 °C, plates were examined at 540 nm using a counter ELX800 (Bio TEK Instruments). Experiments were conducted in triplicate and were repeated at least three times. The values are expressed as percentage inhibition ±SEM (standard error of mean) of cell adhesion relative to untreated cells.

Cell proliferation. EPCs were seeded on gelatin-coated 24-well plates at 6,000 cells/well. After 4 h adhesion in complete medium, cells were exposed to a serum-free medium supplemented with 20 ng/mL VEGFA containing different compounds at 1 μM concentration. After 24 h, 48 h and 72 h, cell numbers and cell viability were determined using trypan blue exclusion assay. All assays were performed in triplicate and repeated at least three times.

In vitro kinase assay. Evaluation of the effects of compound **3** on the kinase activity of human recombinant PDGFRβ and VEGFR2 was performed by measuring the phosphorylation of the substrates Ulight-PolyGAT[EAY(1:1:1)]$_n$ or Ulight-CAGAGAIETDKEYYTVKD (JAK1), respectively, using human recombinant enzymes and the LANCE detection method,[65] employing the Cerep kinase assays.[66]

Western blotting analysis. EPCs were grown in standard condition for 24 h and then exposed to different compounds at 1 μM concentration in a serum and growth factor free medium. After 1 h incubation, cells were treated with 20 ng/mL VEGF-A for 5 min. Next, EPCs were washed twice with ice cold PBS containing 1 mM Na_4VO_3, and lysed in 100 μL of RIPA lysis buffer (#20-188, Millipore) containing 100 μM PMSF and 100 μM OVA and protease inhibitor cocktail-I (#20-201, Millipore). Aliquots of supernatants containing equal amounts of protein in LDS sample buffer (iBlot) were separated on 4-12% (Bis-Tris Plus Blot, Invitrogen). Transfer of fractionated proteins from the gel to a PVDF membrane (iBlot PVDF, Invitrogen) was performed using iBlot system (Invitrogen). Membranes were then blocked with Fluorescent Blocker (Millipore) 1:1 diluted in PBS for 1 h at room temperature. Subsequently, the membrane was probed at 4 °C overnight with 1:1000 rabbit anti-phosphotyrosine-VEGFR2 (#2471 anti-pTyr951, Cell Signaling) or with 1:1000 rabbit anti-VEGFR2 (#441053G, Invitrogen). The membrane was washed in T-PBS buffer, and incubated for 1 h at room temperature with goat anti-rabbit IgG Alexa Flour 750 antibodies (Invitrogen). Immunoreactive bands were visualized by an Odyssey Infrared Imaging System (LI-COR Bioscience). Mouse anti-alpha-tubulin mouse monoclonal antibody (Sigma)/goat anti-mouse IgG Alexa Flour 680 antibodies (Invitrogen), were used to assess equal amount of protein loaded in each lane.

In vitro angiogenesis assay. The effects of the different compounds on the ability of EPCs to reorganize and differentiate into capillary-like network were assessed by Matrigel morphogenesis assay. Briefly, 50 μL of Matrigel matrix growth factor reduced (0.96 mg/mL) was added into wells of a 96-well plate and polymerized for 1 h at 37 °C. Endothelial cells, after 24 h of incubation in standard EGM-2 medium, were washed once with PBS, harvested by trypsinization, and collected by centrifugation. Then, cells were resuspended in 200 μL of

serum/growth factor free EGM-2 medium containing VEGF-A (20ng/mL) and different concentrations of compounds and placed into Matrigel-coated wells (7×10^4 EPC/well). Cells diluted in EGM- 2 basal medium supplemented with VEGF 20 ng/mL were used as positive control. After 6 h incubation on Matrigel at 37 °C, the plates were photographed under a phase contrast microscope and the degree of tubule formation was quantified. The honeycomb pattern is the combination of a series of nodes connected together by branches surrounding enclosed tissues (meshes or loops), thus for quantification of capillary network, the number of loops in four randomly chosen fields from each well was counted. Each experiment was carried out in triplicate.

In vivo angiogenesis assay. Female FVB mice were subcutaneously implanted in both flanks with 0.4 mL of the EHS-derived basement membrane matrix Matrigel (BD Bioscience) which contains types IV collagen, proteoglycans and laminin. Matrigel plugs were added with heparin (5000 U/mL) and VEGF-A (50 ng/mL). Mice were i.p injected every day with 10 mg/kg of sunitinib alone, or equivalent quantity within compound **8**, sunitinib plus **8**, or compound **3**. After 4 days, mice were sacrificed, Matrigel plugs were removed and processed for microscopy investigations.

ASSOCIATED CONTENT

Supporting Information Available: Synthesis of linkers, sunitinib and peptide intermediates and c(AmpRGD)-fluorescein conjugate, HPLC-UV-Vis, HPLC-ESI-MS/MS, flow cytofluorimetry, cell uptake studies, ^{1}H NMR spectra of compounds **1**-**3**, molecular formula strings. This material is available free of charge via the Internet at http://pubs.acs.org.

AUTHOR INFORMATION

Corresponding Authors

* For F. B.: phone, 00390552751310; e-mail: francesca.bianchini@unifi.it

*For F. Z.: phone, 00390521905067; e-mail: franca.zanardi@unipr.it

Author Contributions

The manuscript was written through contributions of all authors. All authors have given approval to the final version of the manuscript.

ACKNOWLEDGMENTS

This work was supported by Ministero dell'Istruzione, dell'Università e della Ricerca (MIUR, PRIN 2010–2011, Protocol No. 2010NRREPL_006), the Istituto Toscano Tumori (ITT) (Grant No. 7197 29/12/2009) and Ente Cassa di Risparmio di Firenze (Protocol No. 2013.0688). Thanks are due to Dr. Valentina Beatrizzotti and Dr. Miriam Girardini (University of Parma) for some synthesis experiments.

ABBREVIATIONS

Amp, 4-amino-L-proline; Boc, *tert*-butoxycarbonyl; Pmc, 2,2,5,7,8-pentamethylchroman-6-sulfonyl; Fmoc, 9-fluorenylmethoxycarbonyl; SPPS, solid phase peptide synthesis; 1,2-DCE, 1,2-dichloroethane; DCM, dichloromethane; DMF, *N*,*N*-dimethylformamide; DIPEA, diisopropylethylamine; TFA, trifluoroacetic acid; TFE, trifluoroethanol; HATU, *O*-(7-azabenzotriazol-1-yl)-*N*,*N*,*N*',*N*'-tetramethyluronium hexafluorophosphate; HOAt, 1-hydroxy-7-azabenzotriazole; BOP, (benzotriazol-1-yloxy)tris(dimethylamino)phosphonium

hexafluorophosphate; TIS, triisopropylsilane; DMAP, 4-(dimethylamino)pyridine; Na L-Asc, (+)-sodium L-ascorbate.

REFERENCES

1. Lammers, T.; Kiessling, F.; Hennink, W. E.; Storm, G. Drug targeting to tumors: principles, pitfalls and (pre-)clinical progress. *J. Control. Release* **2012**, *161*, 175-187.
2. Svensen, N.; Walton, J. G. A.; Bradley, M. Peptides for cell-selective drug delivery. *Trends Pharmacol. Sci.* **2012**, *33*, 186-192.
3. Krall, N.; Scheuermann, J.; Neri, D. Small targeted cytotoxics: current state and promises from DNA-encoded chemical libraries. *Angew. Chem. Int. Ed.* **2013**, *52*, 1384-1402.
4. Hopkins, A. L. Network pharmacology: the next paradigm in drug discovery. *Nat. Chem. Biol.* **2008**, *4*, 682-690.
5. Dar, A. C.; Das, T. K.; Shokat, K. M.; Cagan, R. L. Chemical genetic discovery of targets and anti-targets for cancer polypharmacology. *Nature* **2012**, *486*, 80-84.
6. Daydé-Cazals, B.; Fauvel, B.; Singer, M.; Feneyrolles, C.; Bestgen, B.; Gassiot, F.; Spenlinhauer, A.; Warnault, P.; Van Hijfte, N.; Borjini, N.; Chevé, G.; Yasri, A. Rational design, synthesis, and biological evaluation of 7-azaindole derivatives as potent focused multi-targeted kinase inhibitors. *J. Med. Chem.* **2016**, *59*, 3886-3905.
7. Hanahan, D.; Folkman, J. Patterns and emerging mechanisms of the antiangiogenic switch during tumorigenesis. *Cell* **1996**, *86*, 353-364.
8. Ferrara, N.; Kerbel, R. S. Angiogenesis as a therapeutic target. *Nature* **2005**, *438*, 967-974.
9. Folkman, J. Angiogenesis: an organizing principle for drug discovery? *Nat. Rev. Drug Discov.* **2007**, *6*, 273-286.

10. Weis, S. M.; Cheresh, D. A. Tumor angiogenesis: molecular pathways and therapeutic targets. *Nat. Med.* **2011**, *17*, 1359-1370.
11. Carmeliet, P.; Jain, R. K. Molecular mechanisms and clinical applications of angiogenesis. *Nature* **2011**, *473*, 298-307.
12. Prokopiou, E. M.; Ryder, S. A.; Walsh, J. J. Tumour vasculature targeting agents in hybrid/conjugate drugs. *Angiogenesis* **2013**, *16*, 503-524.
13. Sun, L.; Liang, C.; Shirazian, S.; Zhou, Y.; Miller, T.; Cui, J.; Fukuda, J. Y.; Chu, J.-Y.; Nematalla, A.; Wang, X.; Chen, H.; Sistla, A.; Luu, T. C.; Tang, F.; Wei, J.; Tang, C. Discovery of 5-[5-fluoro-2-oxo-1,2-dihydroindol-(3*Z*)-ylidenemethyl]-2,4-dimethyl-1*H*-pyrrole-3-carboxylic acid (2-diethylaminoethyl)amide, a novel tyrosine kinase inhibitor targeting vascular endothelial and platelet-derived growth factor receptor tyrosine kinase. *J. Med. Chem.* **2003**, *46*, 1116-1119.
14. Faivre, S.; Demetri, G.; Sargent, W.; Raymond, E. Molecular basis for sunitinib efficacy and future clinical development. *Nat. Rev. Drug Discov.* **2007**, *6*, 734-745.
15. Raymond, E.; Dahan, L.; Raoul, J.-L.; Bang, Y.-J.; Borbath, I.; Lomabrd-Bohas, C.; Valle, J.; Metrakos, P.; Smith, D.; Vinik, A.; Chen, J.-S.; Hörsch, D.; Hammel, P.; Wiedenmann, B.; Van Cutsem, E.; Patyna, S.; Lu, D. R.; Blanckmeister, C.; Chao, R.; Ruszniewski, P. Sunitinib malate for the treatment of pancreatic neuroendocrine tumors. *N. Engl. J. Med.* **2011**, *364*, 501-513.
16. Bagcchi, S. Sunitinib still first-line therapy for metastatic renal cancer. *Lancet Oncol.* **2014**, *15*, e420.
17. NIH clinical trials of sunitinib: https://clinicaltrials.gov/ct2/ (August 22, 2016). Very recently, sunitinib was found to be a potent acetylcholinesterase (AChE) inhibitor with

activity in attenuating cognitive impairments in mice. See: Huang, L.; Lin, J.; Xiang, S.; Zhao, K.; Yu, J.; Zheng, J.; Xu, D.; Nirasha, S.; Wang, C.; Chen. X.; Zhang, J.; Xu, S.; Wei, X.; Zhang, Z.; Zhou, D.; Han, Y.; Zhou, W.; Cui, W.; Hu, Z.; Wang, Q. Sunitinib, a clinically anticancer drug, is a potent AChE inhibitor and attenuates cognitive impairments in mice. *ACS Chem Neurosci.* **2016**, *7*, 1047-1056.

18. Mas-Moruno, C.; Rechenmacher, F.; Kessler, H. Cilengitide: the first anti-angiogenic small molecule drug candidate. Design, synthesis and clinical evaluation. *Anti-Cancer Agent Me.* **2010**, *10*, 753-768.
19. Stupp, R.; Hegi, M. E.; Gorlia, T.; Erridge, S. C.; Perry, J.; Hong, Y.-K.; Aldape, K. D.; Lhermitte, B.; Pietsch, T.; Grujicic, D.; Steinbach, J. P.; Wick, W.; Tarnawski, R.; Nam, D.-H.; Hau, P.; Weyerbrock, A.; Taphoorn, M. J. B.; Shen, C.-C.; Rao, N.; Thurzo, L.; Herrlinger, U.; Gupta, T. Cilengitide combined with standard treatment for patients with newly diagnosed glioblastoma with methylated MGMT promoter (CENTRIC EORTC 26071-22072 study): a multicenter, randomized, open-label, phase 3 trial. *Lancet Oncol.* **2014**, *15*, 1100-1108.
20. O'Donnel, P. H.; Karovic, S.; Karrison, T. G.; Janisch, L.; Levine, M. R.; Harris, P. J.; Polite, B. N.; Cohen, E. E. W.; Fleming, G. F.; Ratain, M. J.; Maitland, M. L. Serum C-telopeptide collagen crosslinks and plasma soluble VEGFR2 as pharmacodynamics biomarkers in a trial of sequentially administered sunitinib and cilengitide. *Clin. Cancer Res.* **2015**, *21*, 5092-5099.
21. Vansteenkiste, J.; Barlesi, F.; Waller, C. F.; Bennouna, J.; Gridelli, C.; Goekkurt, E.; Verhoeven, D.; Szczesna, A.; Feurer, M.; Milanowski, J.; Germonpre, P.; Lena, H.; Atanackovic, D.; Krzakowski, M.; Hickling, C.; Straub, J.; Picard, M.; Schuette, W.;

O'Byrne, K. Cilengitide combined with cetuximab and platinum-based chemotherapy as first-line treatment in advanced non-small-cell lung cancer (NSCLC) patients: results of an open-label, randomized, controlled phase II study (CERTO). *Ann. Oncol.* **2015**, *26*, 1734-1740.

22. Jain, R. K. Antiangiogenesis strategies revisited: from starving tumors to alleviating hypoxia. *Cancer Cell* **2014**, *26*, 605-622.
23. https://www.uptodate.com/contents/toxicity-of-molecularly-targeted-antiangiogenic-agents-cardiovascular-effects (August 22, 2016).
24. https://www.uptodate.com/contents/toxicity-of-molecularly-targeted-antiangiogenic-agents-non-cardiovascular-effects (August 22, 2016).
25. Bergers, G.; Hanahan, D. Modes of resistance to anti-angiogenic therapy. *Nat. Rev. Cancer* **2008**, *8*, 592-603.
26. Francia, G.; Emmenegger, U.; Kerbel, R. S. Tumor-associated fibroblasts as "Trojan horse" mediators of resistance to anti-VEGF therapy. *Cancer Cell* **2009**, *15*, 3-5.
27. Ebos, J. M. L.; Lee, C. R.; Cruz-Munoz, W.; Bjarnason, G. A.; Christensen, J. G.; Kerbel, R. S. Accelerated metastasis after short-term treatment with a potent inhibitor of tumor angiogenesis. *Cancer Cell* **2009**, *15*, 232-239.
28. Gotink, K. J.; Broxterman, H. J.; Labots, M.; de Haas, R. R.; Dekker, H.; Honeywell, R. J.; Rudek, M. A.; Beerepoot, L. V.; Musters, R. J.; Jansen, G.; Griffioen, A. W.; Assaraf, Y. G.; Pili, R.; Peters, G. J.; Verheul, H. M. W. Lysosomal sequestration of sunitinib: a novel mechanism of drug resistance. *Clin. Cancer Res.* **2011**, *17*, 7337-7346.
29. Gacche, R. N. Compensatory angiogenesis and tumor refractoriness. *Oncogenesis* **2015**, *4*, e153.

30. El-Kenawi, A. E.; El-Remessy, A. B. Angiogenesis inhibitors in cancer therapy: mechanistic perspective on classification and treatment rationales. *Brit. J. Pharmacol.* **2013**, *170*, 712-729.
31. Reynolds, A. R.; Reynolds, L. E.; Nagel, T. E.; Lively, J. C.; Robinson, S. D.; Hicklin, D. J.; Bodary, S. C.; Hodivala-Dilke, K. M. Elevated Flk1 (vascular endothelial growth factor receptor 2) signaling mediates enhanced angiogenesis in beta3-integrin-deficient mice. *Cancer Res.* **2004**, *64*, 8643-8650.
32. Mahabeleshwar, G. H.; Feng, W.; Phillips, D. R.; Byzova, T. V. Integrin signaling is critical for pathological angiogenesis. *J. Exp. Med.* **2006**, *203*, 2495-2507.
33. Mahabeleshwar, G. H.; Feng, W.; Reddy, K.; Plow, E. F.; Byzova, T. V. Mechanisms of integrin-vascular endothelial growth factor receptor cross-activation in angiogenesis. *Circ. Res.* **2007**, *101*, 570-580.
34. Mahabeleshwar, G. H.; Chen, J.; Feng, W.; Somanath, P. R.; Razorenova, O. V.; Byzova, T. V. Integrin affinity modulation in angiogenesis. *Cell Cycle* **2008**, *7*, 335-347.
35. Somanath, P. R.; Malinin, N. L.; Byzova, T. V. Cooperation between integrin $\alpha_V\beta_3$ and VEGFR2 in angiogenesis. *Angiogenesis* **2009**, *12*, 177-185.
36. Robinson, S. D.; Hodivala-Dilke, K. M. The role of β_3-integrins in tumor angiogenesis: context is everything. *Curr. Opin. Cell Biol.* **2011**, *23*, 630-637.
37. Strieth, S.; Eichhorn, M. E.; Sutter, A.; Jonczyk, A.; Berghaus, A.; Dellian, M. Antiangiogenic combination tumor therapy blocking α_V-integrins and VEGF-receptor-2 increases therapeutic effects *in vivo*. *Int. J. Cancer* **2006**, *119*, 423-431.

38. Papo, N.; Silverman, A. P.; Lahti, J. L.; Cochran, J. R. Antagonistic VEGF variants engineered to simultaneously bind to and inhibit VEGFR2 and $\alpha_V\beta_3$ integrin. *Proc. Natl. Acad. Sci.* **2011**, *108*, 14067-14072.

39. Kim, T. J.; Landen, C: N.; Lin, Y. G.; Mangal, L. S.; Lu, C.; Nick, A. M.; Stone, R. L.; Merritt, W. M.; Armaiz-Pena, G.; Jennings, N. B.; Coleman, R. L.; Tice, D. A.; Sood, A. K. Combined anti-angiogenic therapy against VEGF and integrin $\alpha_V\beta_3$ in an orthotopic model of ovarian cancer. *Cancer Biol. Ther.* **2009**, *8*, 2261-2270.

40. Zanella, S.; Mingozzi, M.; Dal Corso, A.; Fanelli, R.: Arosio, D.; Cosentino, M.; Schembri, L.; Marino, F.; De Zotti, M.; Formaggio, F.; Pignataro, L.; Belvisi, L.; Piarulli, U.; Gennari, C. Synthesis, characterization, and biological evaluation of a dual-action ligand targeting $\alpha_V\beta_3$ integrin and VEGF receptors. *ChemistryOpen* **2015**, *4*, 633-641.

41. Zanardi, F.; Burreddu, P.; Rassu, G.; Auzzas, L.; Battistini, L.; Curti, C.; Sartori, A.; Nicastro, G.; Menchi, G.; Cini, N.; Bottoncetti, A.; Raspanti, S.; Casiraghi, G. Discovery of subnanomolar arginine-glycine-aspartate-based $\alpha_V\beta_3/\alpha_V\beta_5$ integrin binders embedding 4-aminoproline residues. *J. Med. Chem.* **2008**, *51*, 1771-1782 (corrigendum *J. Med. Chem.* **2008**, *51*, 2870).

42. Battistini, L.; Burreddu, P.; Carta, P.; Rassu, G.; Auzzas, L.; Curti, C.; Zanardi, F.; Manzoni, L.; Araldi, E. M. V.; Scolastico, C.; Casiraghi, G. 4-Aminoproline-based arginine-glycine-aspartate integrin binders with exposed ligation points: practical in-solution synthesis, conjugation and binding affinity evaluation. *Org. Biomol. Chem.* **2009**, *7*, 4924-4935.

43. Sartori, A.; Bianchini, F.; Migliari, S.; Burreddu, P.; Curti, C.; Vacondio, F.; Arosio, D.; Ruffini, L.; Rassu, G.; Calorini, L.; Pupi, A.; Zanardi, F.; Battistini, L. Synthesis and

preclinical evaluation of a novel, selective ^{111}In-labelled aminoproline-RGD-peptide for non-invasive melanoma tumor imaging. *Med. Chem. Commun*. **2015**, *6*, 2175-2183.

44. For an example of cell-selective sunitinib-like/platinum(II) bioconjugate with multikinase inhibitory activity, see: Harmsen, S.; Dolman, M. E. M.; Nemes, Z.; Lacombe, M.; Szokol, B.; Pató, J.; Kéri, G.; Orfi, L.; Storm, G.; Hennink, W. E.; Kok, R. J. Development of a cell-selective and intrinsically active multikinase inhibitor bioconjugate. *Bioconj. Chem.* **2011**, *22*, 540-545.
45. For an example of targeted liposome-mediated delivery of sunitinib, see: Shi, J.-F.; Sun, M.-G.; Li, X.-Y.; Zhao, Y.; Ju, R.-J.; Mu, L.-M.; Yan, Y.; Li, X.-T.; Zeng, F.; Lu, W.-L. A combination of targeted sunitinib liposomes and targeted vinorelbine liposomes for treating invasive breast cancer. *J. Biomed. Nanotech.* **2015**, *11*, 1568-1582.
46. Very recently, the synthesis and preclinical studies of one GnRH-sunitinib succinate-linked conjugate was reported, which was proven to selectively reach prostate cancer site and downregulate angiogenesis. See: Argyros, O.; Karampelas, T.; Asvos, X.; Varela, A.; Sayyad, N.; Papakyriakou, A.; Davos, C. H.; Tzakos, A. G.; Fokas, D.; Tamvakopoulos, C. Peptide-drug conjugate GnRH-sunitinib targets angiogenesis selectively at the site of action to inhibit tumor growth. *Cancer Res.* **2016**, *76*, 1181-1192.
47. Musumeci, F.; Radi, M.; Brullo, C.; Schenone, S. Vascular endothelial growth factor (VEGF) receptors: drugs and new inhibitors. *J. Med. Chem.* **2012**, *55*, 10797-10822.
48. McTigue, M.; Murray, B. W.; Chen, J. C.; Deng, Y.-L.; Solowiej, J.; Kania, R. S. Molecular conformations, interactions, and properties associated with drug efficiency and clinical performance among VEGFR TK inhibitors. *Proc. Natl. Acad. Sci.* **2012**, *109*, 18281-18289.

49. Capelli, A. M.; Costantino, G. Unbinding pathways of VEGFR2 inhibitors revealed by steered molecular dynamics. *J. Chem. Inf. Model.* **2014**, *54*, 3124-3136.

50. Pilkington-Miksa, M.; Arosio, D.; Battistini, L.; Belvisi, L.; De Matteo, M.; Vasile, F.; Burreddu, P.; Carta, P.; Rassu, G.; Perego, P.; Carenini, N.; Zunino, F.; De Cesare, M.; Castiglioni, V.; Scanziani, E.; Scolastico, C.; Casiraghi, G.; Zanardi, F.; Manzoni L. Design, synthesis and biological evaluation of novel cRGD-paclitaxel conjugates for integrin-assisted drug delivery. *Bioconj. Chem.* **2012**, *23*, 1610-1622.

51. Battistini, L.; Burreddu, P.; Sartori, A.; Arosio, D.; Manzoni, L.; Paduano, L.; D'Errico, G.; Sala, R.; Reia, L.; Bonomini, S.; Rassu, G.; Zanardi, F. Enhancement of the uptake and cytotoxic activity of doxorubicin in cancer cells by novel cRGD-semipeptide-anchoring liposomes. *Mol. Pharm.* **2014**, *11*, 2280-2293.

52. Boturyn, D.; Coll, J.-L.; Garanger, E.; Favrot, M.-C.; Dumy, P. Template assembled cyclopeptides as multimeric system for integrin targeting and endocytosis. *J. Am. Chem. Soc.* **2004**, *126*, 5730-5739.

53. Dijkgraaf, I.; Kruijtzer, J. A.; Liu, S.; Soede, A. C.; Oyen, W. J. G.; Corstens, F. H.; Liskamp, R. M.; Boerman, O. C. Improved targeting of the $\alpha_v\beta_3$ integrin by multimerization of RGD peptides. *Eur. J. Nucl. Med. Mol. Imaging* **2007**, *34*, 267-273.

54. Liu, S. Radiolabeled RGD peptides as integrin $\alpha_v\beta_3$-targeted radiotracers: maximizing binding affinity via bivalency. *Bioconj. Chem.* **2009**, *20*, 2199-2213.

55. Sancey, L.; Garanger, E.; Foillard, S.; Schoehn, G.; Hurbin, A.; Albiges-Rizo, C.; Boturyn, D.; Souchier, C.; Grichine, A.; Dumy, P.; Coll, J.-L. Clustering and internalization of integrin $\alpha_v\beta_3$ with a tetrameric RGD-synthetic peptide. *Mol. Ther.* **2009**, *17*, 837-843.

56. Ivaska, J.; Heino, J. Cooperation between integrins and growth factor receptors in signaling and endocytosis. *Annu. Rev. Cell Dev. Biol.* **2011**, *27*, 291-320.

57. Liu, S. Radiolabeled cyclic RGD peptide bioconjugates as radiotracers targeting multiple integrins. *Bioconj. Chem.* **2015**, *26*, 1413-1438.

58. The photoinduced *Z-E* isomerization of sunitinib drug is reknown as it is known that dark conditions promote reversible re-conversion to the biologically active *Z*-isomer. In our hands, all "sunitinib-containing" compounds were pure *Z*-configured compounds and were treated under dark conditions to prevent possible isomerization. See: Sistla, A.; Shenoy, N. Reversible *Z-E* isomerism and pharmaceutical implications for SU5416. *Drug Dev. Ind. Pharm*. **2005**, *31*, 1001-1007.

59. Ribatti, D. The involvement of endothelial progenitor cells in tumor angiogenesis. *J. Cell Mol. Med.* **2004**, *8*, 294-300.

60. Marçola, M.; Rodrigues, C. E. Endothelial progenitor cells in tumor angiogenesis: another brick in the wall. *Stem Cells Int.* **2015**, *2015*, 832649.

61. The expression of β_1 integrins (e.g. $\alpha_5\beta_1$) in EPCs was also evaluated; it was determined to be about 35-40%, lower than the expression of $\alpha_V\beta_3$ (>87.5%).

62. Chen, P. Y.; Qin, L.; Zhuang, Z. W.; Tellides, G.; Lax, I.; Schlessinger, J.; Simons, M. The docking protein FRS2α is a critical regulator of VEGF receptors signaling. *Proc. Natl. Acad. Sci. U S A.* **2014**, *111*, 5514-5519.

63. Margheri, F., Killa, A.; Laurenzana, A.; Serrati, S.; Mazzanti, B.; Saccardi, R.; Santosuosso, M.; Danza, G.; Sturli, N.; Rosati, F.; Magnelli, L.; Papucci, L.; Calorini, L.; Bianchini, F.; Del, R. M.; Fibbi, G. Endothelial progenitor cell-dependent angiogenesis

requires localization of the full-length form of uPAR in caveolae. *Blood* **2011**, *118*, 3743-3755.

64. Carmi, C.; Galvani, E.; Vacondio, F.; Rivara, S.; Lodola, A.; Russo, S.; Aiello, S.; Bordi, F.; Costantino, G.; Cavazzoni, A.; Alfieri, R.R.; Ardizzoni, A.; Petronini, P. G.; Mor, M. Irreversible inhibition of epidermal growth factor receptor activity by 3-aminopropanamides. *J. Med. Chem.* **2012**, *55*, 2251-2264.
65. Olive, D. M. Quantitative methods for the analysis of protein phosphorylation in drug development. *Expert Rev. Proteomics* **2004**, *1*, 327−341.
66. CEREP, catalogue on line: http://www.cerep.fr/cerep/users/pages/catalog/Affiche_CondExp_Test.asp?test=2900 (for PDGFRβ, November 29, 2016) and http://www.cerep.fr/cerep/users/pages/catalog/Affiche_CondExp_Test.asp?test=2864 (for VEGFR2, November 29, 2016).

Table of Contents Graphic